Role of nanomaterials in water treatment applications: A review

6 authors, including:

Santhosh C.
VIT University
24 PUBLICATIONS **114** CITATIONS

SEE PROFILE

Venugopal Velmurugan
VIT University
24 PUBLICATIONS **63** CITATIONS

SEE PROFILE

Amit Bhatnagar
University of Eastern Finland
119 PUBLICATIONS **4,002** CITATIONS

SEE PROFILE

Review

Role of nanomaterials in water treatment applications: A review

Chella Santhosh [a], Venugopal Velmurugan [b], George Jacob [b], Soon Kwan Jeong [c], Andrews Nirmala Grace [b,*], Amit Bhatnagar [a,*]

[a] Department of Environmental and Biological Sciences, University of Eastern Finland, FI-70211 Kuopio, Finland
[b] Center for Nanotechnology Research, VIT University, Vellore 632014, India
[c] Climate Change Technology Research Division, KIER, Yuseong-gu, Daejeon 305-343, South Korea

HIGHLIGHTS

- Use of nanomaterials (NMs) in water treatment has been reviewed.
- Carbon nanomaterials, nano metal oxides and nano composites are reviewed.
- Adsorption, photocatalytic and antimicrobial properties of NMs are reviewed.

ARTICLE INFO

ABSTRACT

Water pollution by various toxic contaminants has become one of the most serious problems worldwide. Various technologies have been used to treat water and waste water including chemical precipitation, ion-exchange, adsorption, membrane filtration, coagulation–flocculation, flotation and electrochemical methods. From past few decades, nanotechnology has gained wide attention and various nanomaterials have been developed for the water remediation. In the present review article, various nanomaterials have been reviewed which have been used for water decontamination. The special emphasis in the review has been given on adsorption, photocatalytic and antibacterial activity of nanomaterials.

© 2016 Elsevier B.V. All rights reserved.

Contents

1. Introduction

Clean water is one of the most important elements for all living organisms to sustain life. However, due to the rapid pace of industrialization and tremendous increase in the population, the contamination of water resources has occurred globally [1,2]. Besides other needs, the demand for water has increased tremendously in agricultural, industrial and domestic sectors consuming 70, 22 and 8% of the available fresh water, respectively and this has resulted in the generation of large amounts of wastewater [3–5] containing a number of 'pollutants'. Some of the important classes of aquatic pollutants are heavy metal ions and dyes, and once these enter into the water, water is no longer safe for drinking purpose and sometimes it is very difficult to completely treat the contaminated water [6,7]. Aquatic pollutants are often very dangerous for living beings, and also affect the ecosystem. Therefore, the removal of these pollutants from contaminated water is an urgent need in order to prevent the negative effects on the human health and to the environment.

From past few decades, various techniques have been developed for treating the waste water [8–13]. Among them, most important methods are solvent extraction, micro and ultra-filtration, sedimentation and gravity separation, flotation, precipitation, coagulation, oxidation, evaporation, distillation, reverse osmosis, adsorption, ion exchange, electrodialysis, electrolysis, etc. From above mentioned techniques, adsorption is one of the considerable techniques for treating the waste water, because of its easy operation, low cost and the availability of a wide range of adsorbents. Besides, adsorption can also be applied for the removal of soluble and insoluble organic, inorganic, and biological pollutants. Additionally, adsorption can also be used for source reduction and reclamation for potable, industrial, and other water purposes. In spite of these facts, adsorption has certain limitations such as it could not achieve a good status at commercial levels. Probably, it is due to the lack of suitable adsorbents with high adsorption capacity and limited use of adsorbents on commercial scale columns. Besides, a single adsorbent cannot be used for removing all kind of pollutants. Different adsorbents are used for different pollutants based on their properties. A comparison of adsorption method was carried out with other water treatment technologies. The order of cost effectiveness is adsorption > evaporation > aerobic > anaerobic > ion exchange > electrodialysis > micro- and ultra-filtration > reverse osmosis > precipitation > distillation > oxidation > solvent extraction [14]. It was observed that, in spite of some limitations, adsorption will be considered a good water treatment technology in the near future. Much work has been conducted on the removal of different pollutants from water by using adsorption in batch mode process [14,15]. Initially, activated carbon was used for the removal of pollutants from water, which has been replaced by some cost-effective adsorbents [16–18]. In the last two decades, nanotechnology has emerged significantly with its applications in almost all branches of science and technology. As a matter of fact, various nanomaterials have been prepared and used for the removal of aquatic pollutants [19]. In view of the importance of water quality and emerging utilities of nanotechnology, attempts have been made to discuss various aspects of water treatment by adsorption using nanomaterials. In this regard, promoting nanomaterials presents opportunities to develop local and practical solutions for tackling global water pollution. This review article presents a brief overview of the technical applicability of different nanomaterials for removing various aquatic pollutants.

Although many excellent review articles have been published so far discussing the importance of nanomaterials in water treatment and environmental remediation, but some of them are only a material and/or adsorbent-specific (e.g., CNTs, graphene-based nanomaterials, nano metal oxides, nano zerovalent iron, cellulose nanomaterials [20–26]) or an adsorbate specific (e.g., metals [22,24,27], dyes [28], pharmaceuticals and personal care products [29]). One of the aims of the present review is to compile the important findings of different types of nanomaterials, used in water treatment either as adsorbents, photocatalysts and/or antibacterial agents, for the removal of important aquatic pollutants. A summary of relevant published data with some of the latest important findings, and a source of up-to-date literature is presented and the results have been discussed.

2. Nanomaterials as adsorbents for water treatment

Nanoadsorbents are nanoscale particles from organic or inorganic materials that have a high affinity to adsorb substances. Because of their high porosity, small size, and active surface, nanoadsorbents not only are capable of sequestering contaminants with varying molecular size, hydrophobicity, and speciation behavior, but also enable manufacturing process to consume raw materials efficiently without releasing its toxic payload [30]. Nanoadsorbents not only work rapidly, but also have considerable pollutant-binding capacities. They can also be chemically regenerated after being exhausted [31]. For these reasons, scholarly interests of nanotechnology have been growing rapidly worldwide. At the nanoscale, materials show unique characteristics and, because of their small size, they possess a large surface area and 'surface area to volume' ratio [32]. These characteristics improve the adsorption capacity of the nanoparticles. In addition to the large surface area, these particles show unique characteristics, such as catalytic potential and high reactivity, which make them as better adsorbing materials than conventional materials. Because of their high surface area, nanoparticles have a greater number of active sites for interaction with different chemical species [33–35]. To get better results for the removal of pollutants from wastewater, nanoparticles are becoming new alternatives for the treatment of wastewater [36–40].

2.1. Carbon based materials

For any adsorption process, an adsorbent having large surface area, pore volume, and proper functionalities is the key to success. Currently, many different porous materials have been developed, such as activated carbon, pillared clays, zeolites, mesoporous oxides, polymers and metal-organic frameworks, showing varying extent of effectiveness in removing the toxic pollutants from air, water and soil [41–45]. Among them, carbon-based adsorbents including activated carbon, carbon nanotubes, fullerenes and

graphene, usually show high adsorption capacity and thermal stability [46–49]. Of the various nanomaterials based adsorbents, carbon based materials have been probed as superior adsorbents for the removal of inorganic and organic pollutants. Since the discovery of carbon nanotubes (CNTs) and fullerene, these materials have been extensively used as effective adsorbents but its large scale application is limited on economic grounds and hence, designing the adsorbents at a lower cost is a great challenge. Multiwalled carbon nanotube shows considerable removal efficiency of inorganic metal ions with the help of magnetic nanomaterials [50].

2.1.1. Carbon nanotubes (CNTs)

Carbon nanotubes are one of the allotropes of carbon and these can be considered as various structural forms of carbon element. Basically CNTs are composed of cylindrical shape rolled up in a tube like structure. CNTs are of two types, single walled carbon nanotubes (SWCNTs) and multiwalled carbon nanotubes (MWCNTs), where single walled carbon nanotubes are composed of single graphene sheet with a roll up and multiwalled carbon nanotubes are of multiple graphene roll up sheets. Fig. 1 shows the structures of SWCNTs and MWCNTs.

CNTs, with their high surface active site to volume ratio and controlled pore size distribution, have an exceptional sorption capability and high sorption efficiency compared to conventional granular and powder activated carbon, which have intrinsic limitations like surface active sites and the activation energy of sorption.

Extensive studies have found that the adsorption capacity of CNTs depends on both the surface functional groups and the nature of the sorbate. For instance, the amounts of surface acidity (carboxylic, lactonic and phenolic groups) favor the adsorption of polar compounds [51]. On the other hand, unfunctionalized CNT surface is proved to have higher adsorption capacity towards non-polar compounds such as polycyclic aromatic hydrocarbons [52]. The sorption behaviors of CNTs mainly involve chemical interaction for polar compounds and physical interaction for non-polar compounds which is given in Table 1.

Sorption capacity of CNTs is effective over a broad pH range. Particularly, optimum performance was reported in the pH range of 7–10. Other than this pH range, ionization and competition between ionic species could occur. Although CNTs are more expensive compared to conventional activated carbon, their sorption and desorption cycles are more efficient.

Table 1
Heavy metal ions adsorption onto various types of carbon nanotubes.

S. No.	Adsorbents	Metal ions	Adsorption capacity	Refs.
1.	CNTs	Pb^{2+}	17.44 mg/g at pH-7.0	[52]
2.	CNTs (HNO_3)	Pb^{2+}	49.95 mg/g at pH-7.0	[53]
3.	MWCNTs	Ni^{2+}	7.53 mg/g at pH-7.0	[54]
4.	SWCNTs	Ni^{2+}	9.22 mg/g at pH-7.0	[54]
5.	MWCNTs (HNO_3)	Pb^{2+}	97.08 mg/g at pH-5.0	[55]
6.	CNTs	Pb^{2+}	1.406 mmol/g	[56]
7.	CNT–OH	Pb^{2+}	2.07 mmol/g	[56]
8.	CNT–$CONH_2$	Pb^{2+}	1.907 mmol/g	[56]
9.	CNT–COO^-	Pb^{2+}	4.672 mmol/g	[56]
10.	CNTs	Cu^{2+}	1.219 mmol/g	[56]
11.	CNT–OH	Cu^{2+}	1.342 mmol/g	[56]
12.	CNT–$CONH_2$	Cu^{2+}	1.755 mmol/g	[56]
13.	CNT–COO^-	Cu^{2+}	3.565 mmol/g	[56]
14.	CNTs	Cd^{2+}	1.291 mmol/g	[56]
15.	CNT–OH	Cd^{2+}	1.513 mmol/g	[56]
16.	CNT–$CONH_2$	Cd^{2+}	1.563 mmol/g	[56]
17.	CNT–COO^-	Cd^{2+}	3.325 mmol/g	[56]
18.	CNTs	Hg^{2+}	1.068 mmol/g	[56]
19.	CNT–OH	Hg^{2+}	1.284 mmol/g	[56]
20.	CNT–$CONH_2$	Hg^{2+}	1.658 mmol/g	[56]
21.	CNT–COO^-	Hg^{2+}	3.300 mmol/g	[56]

Lu and Chiu [57] discussed the removal of zinc (Zn^{2+}) using purified CNTs (MWCNTs and SWCNTs). As reported in other studies [58], purification resulted in the removal of metal catalysts and amorphous carbon from CNTs and large quantities of nanotube bundles with the hollow inner tube diameter were observed in the purified CNTs. The zeta potentials of purified CNTs were more negative than that of raw CNTs due to the presence of negative functional groups on the surface of purified CNTs. Adsorption of Zn^{2+} was favorable in the pH range of 2.0–12.0. But low Zn^{2+} adsorption occurred at low pH due to the competition between H^+ and Zn^{2+} for the adsorption sites. After an increase in Zn^{2+} adsorption up to pH 8.0, the adsorption remained constant in the pH range of 8.0–11.0. The Zn^{2+} species prevails until pH 8.0, and the process governing the Zn^{2+} removal is adsorption. The kinetics of Zn^{2+} adsorption onto the CNTs was fast (60 min). The maximum adsorption capacities of Zn^{2+} calculated by the Langmuir model were reported as 43.66, and 32.68 mg/g for SWCNTs and MWCNTs, respectively, at an initial Zn^{2+} concentration range of 10–80 mg/L. Gupta et al. [59] studied removal of Cr(III) by combining the
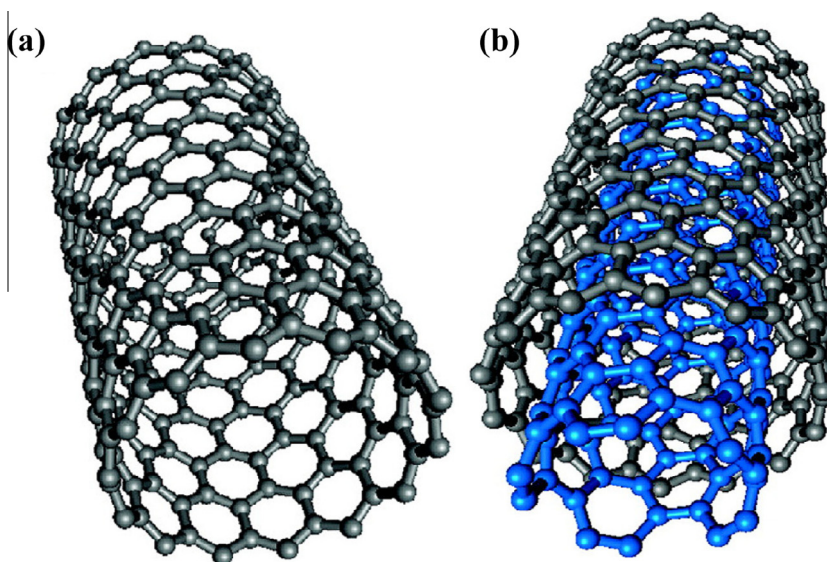

Fig. 1. Structure representations of (a) SWCNTs and (b) MWCNTs.

magnetic properties of iron oxide with adsorption properties of MWCNTs. Acid treatment (HNO_3) of MWCNTs was performed to modify the surface of CNTs with carbonyl and hydroxyl groups. The additional adsorbing sites provided by the oxygen atoms of iron oxide nanoparticles on the surface of MWCNTs became available for the electrostatic interaction with Cr(III) and thus, the prepared composite showed higher capacity for Cr(III). The composite was effective for Cr(III) adsorption in the pH range of 3.0–7.0 due to the presence of $Cr(OH)^{2+}$ species of chromium at pH 4.0–7.0. Also, at pH values of 4.0–7.0, the net negative surface charge on the former allowed increased adsorption of chromium species on MWCNTs. The results of the fixed bed experiments revealed that lower flow rate favored Cr(III) removal due to the increased contact time between Cr(III) and adsorbent. Increase in fixed bed layers also revealed an increase in Cr(III) uptake which was attributed to the availability of more adsorption sites. Several researchers have also modified the carbon nanotubes to evaluate the efficiency of the former with the unmodified CNTs for the removal of various contaminants [46,47].

Wu [60] evaluated the performance of carbon nanotubes (MMWCNTs) for the adsorption of Procion Red MX-5B dye which is present in various industrial effluents. The kinetic analysis at different temperature was evaluated at pH 6.5. The maximum adsorption capacity was achieved within 3 h at various temperatures 281, 291, 301 and 321 K was 20.93, 22.87, 27.20 and 30.53 mg/g, respectively. Temperature also favored the adsorption of Procion Red MX-5B onto dye carbon nanotubes. The adsorption increased with temperature, indicating that the mobility of dye molecules increased with temperature, as did the number of molecules that interact with the active sites at CNTs; moreover, the adsorption was endothermic. The linear correlation coefficients and standard deviations of Langmuir and Freundlich isotherms were determined and the results revealed that Langmuir isotherm fitted the experimental results well. Kinetic analyses were conducted using pseudo first and pseudo second-order models and the intra particle diffusion model. The regression results showed that the adsorption kinetics was more accurately represented by a pseudo second-order model. Changes in the free energy of adsorption (G°), enthalpy (H°) and entropy (S°), as well as the activation energy (E_a) were determined. H° and S° were found to be 31.55 kJ/mol and 216.99 J/mol K, respectively, at pH 6.5 and 41.47 kJ/mol and 244.64 J/mol K at pH 10. The activation energy was 33.35 kJ/mol at pH 6.5. Thermodynamic parameters suggested that the adsorption of Procion Red MX-5B dye onto CNTs was physisorption.

Chatterjee et al. [61] impregnated chitosan (CS) hydrogel beads with multi-walled carbon nano tubes (CNTs) and studied the adsorption efficiency of modified adsorbent for Congo red (CR) dye removal. The CNT impregnation rendered the beads materially denser and the porosity of the CS/CNT beads also increased due to the addition of CNT. The adsorption of CR onto CS/CNT was highly pH dependent and maximum adsorption (423.1 mg/g) by the CS/CNT beads occurred at pH 4.0. Since the beads formation was conducted in a sodium hydroxide precipitation bath, the amine groups of CS molecules were not protonated. An increase in initial pH 4.0–5.6 and from pH 5.0–6.0 during adsorption indicated a decrease in H^+ concentration in the solution. Although such behavior was absent when the initial pH of the CR solution was neutral or basic as protonation of amine groups did not occur at pH 7.0 and 9.0 due to the absence of free H^+ in solution. The Langmuir isotherm model showed better fit to the experimental isotherm data than the Freundlich isotherm model. The maximum adsorption capacity of CS/CNT beads for CR was reported as 450.4 mg/g. The values obtained from pseudo-first order, pseudo-second order kinetic models and intra-particle diffusion model showed that the mass transfer rate was fairly increased by the addition of CNT. Bazrafshan et al. [62]

studied the removal of reactive red 120 textile dye (RR-120) using SWCNTs. The adsorptive removal of RR-120 was influenced by pH. The optimum pH for the process was 5.0 as below and above this pH, adsorptive removal of the dye was found to decrease. Maximum adsorption capacity of SWCNTs for the dye was reported as 426.49 mg/g with 85.3% dye removal taking place at pH 5.0 with initial dye concentration of 50 mg/L. The increased adsorbent dosage resulted in the increase in surface area and adsorption sites helped in achieving maximum dye adsorption (88.28%, 882.83 mg/g). Adsorption equilibrium was achieved in 180 min contact time. The BET model fitted well to the isotherm data.

In another study, resorcinol was taken as a model phenolic derivative and the efficiency of MWCNTs was assessed for the adsorption of resorcinol [63]. The kinetics of resorcinol onto MWCNTs was fast. The experiments were not performed at pH values greater than 8.0 as in basic condition resorcinol is oxidized. Resorcinol uptake increased with the decrease in solution pH since its solubility decreases with the lowering of pH. A reduction in the uptake capacity of resorcinol was observed due to the electrostatic repulsion between negatively charged resorcinol and acid-treated MWCNTs. Also the carboxylic groups, those were present on the surface of MWCNTs, acted as electrons withdrawing groups localizing electron from π system of MWCNTs interfering and weakening the forces between aromatic ring of resorcinol and graphite structure of MWCNTs. The hydroxyl group (located in *meta*-position) present in the structure of resorcinol also positively influenced its adsorption. The potential of MWCNTs for herbicide adsorption has also been tested by the researchers [64].

Carbon nanotubes have also been tested for the removal of natural organic matter (NOM) from aqueous solution and the results have been found promising. Hyung and Kim [65] investigated the role of MWCNTs in the removal of NOM. CNT in particular, in the natural aquatic environment might occur to a higher extent than predicted based only on the hydrophobicity of these materials. The NOM had anionic character across the pH range 3.0–9.0. The effect of NOM characteristics and water quality parameters on adsorptive interaction between MWCNT and NOM in aqueous phase was examined. Freundlich isotherm studies have been employed and were compared with the adsorption onto activated carbon. Finally, the amount of stable MWCNT suspension formed in water as a result of NOM adsorption under varying conditions was quantitatively analyzed. A wide range of NOM concentrations (2.5–50 mg C/L) was investigated, and it was noted that NOM concentrations in some natural surface and ground waters were lower than concentration levels used. Joseph et al. [66] investigated NOM removal from a variety of potential drinking water sources through a combination of coagulation and adsorption with CNTs. Both SWCNTs and MWCNTs were examined for their removal efficiencies for NOM parallel to coagulation process in the presence of alum and ferric chloride metal coagulants. Synthetic seawater (SW) and brackish water (BW) (contained humic acid as its representative NOM), synthetic (old and young) landfill leachates (OL, YL) (contained glucose as its representative NOM), and natural river water (BRW) were chosen to obtain a detailed knowledge of NOM and its behavior towards adsorption and coagulation. Humic acid used in the study contained ~40% DOC. The isotherm data of BW, SW and BRW fitted well with the Freundlich model and SWCNTs consistently had a higher adsorption capacity than MWCNTs for NOM. The higher specific surface area of SWCNTs (407 m^2/g) as compared to that of MWCNTs (60 m^2/g) was attributed to be responsible for the greater NOM uptake capacity of former.

Adsorption of trihalomethanes (THMs) from water using MWCNTs has also been investigated [67]. Multiwalled carbon nanotubes (MWCNTs) were purified by mixed HNO_3/H_2SO_4 solution and were employed as adsorbents. THM solution consisted of

equivalent concentrations of $CHCl_3$, $CHCl_2Br$, $CHClBr_2$, and $CHBr_3$. The kinetic studies showed that diffusion mechanism controlled the THMs adsorption onto CNTs and the smallest molecule, $CHCl_3$ was preferred over other THMs ($CHCl_2Br$, $CHClBr_2$, and $CHBr_3$) because $CHCl_3$ could easily enter the inner cavities through the pores. The adsorption capacity of $CHCl_3$ was observed to be the highest (3.158 mg/g), followed by $CHBrCl_2$ (2.016 mg/g), $CHBr_2Cl$ (2.008 mg/g) and then $CHBr_3$ (1.976 mg/g) at 5 °C. As the temperature increased from 5 °C to 35 °C, there was a decrease in the adsorption capacities as well. Furthermore, the adsorption capacity of THM molecules onto CNTs from a pure solution was found to be quite different from a mixed solution. As the temperature increased from 5 to 35 °C, the maximum adsorption capacity of $CHCl_3$ calculated by the Langmuir model decreased from 3.158 to 2.826 mg/g. These values were two to three times more than that of commercially available PAC (1.32 mg/g) measured at 25 °C in the study, reflecting that CNTs are efficient adsorbents. The kinetics of adsorption process was found to follow the first order rate law. Morawski et al. [68] indicated that the adsorption of $CHCl_3$ onto carbon sphere from a mixed solution was strongly depressed, about 40% of adsorption capacity from a solution of pure $CHCl_3$. Besides these, several other reports are available where carbon nanomaterials have been used for the removal of aquatic pollutants [69–71].

There is no doubt that CNTs possess great potential as superior adsorbents for removing divalent metal ions, dyes, NOMs and THMs from aqueous solution, but their relatively high unit cost restricts their practical use. In addition to it, raw CNTs may possess some degree of toxicity due to the presence of metal catalysts while chemically functionalized CNTs have not demonstrated any toxicity so far [72]. As a result, the practical use of CNTs as sorbents in water and wastewater treatment depends on the continuation of research into the development of a cost effective way of CNTs production and the no or low toxicity of CNTs and CNT related materials such as carbon nanocrystals (CNCs).

Besides metals removal, CNTs have also been used for the removal of various organic pollutants from water and wastewater and a brief discussion is presented here. Most of the organic dyes will have high levels of toxicity at their lower level of concentration in water and will affect the potential carcinogenic effects in the living organisms. Due to these reason, most of the researchers are working on the treatment of organic dyes using various adsorbents, before leaving them into the environment. For treating the organic dyes from wastewaters, there are wide range of adsorbents

has been used, such as zeolites, clays, polymers and activated carbon, etc., Dyes are important water pollutants which are generally present in the effluents of the textile, leather, food processing, dyeing, cosmetics, paper, and dye manufacturing industries. The colored dye effluents are generally considered to be highly toxic to the aquatic biota and affect the symbiotic process by disturbing the natural equilibrium through reduced photosynthetic activity due to the coloration of the water in streams. Carbon nanotubes are one of the promising adsorbent for treating the organic dyes, because of their large surface area and their unique properties [73,74]. Other than dyes, some other organic pollutants such as pharmaceuticals, phenols, pesticides, aromatic amines, and other toxic organics have shown the potential negative impact on the environment, mainly onto the water sources. For example, olaquindox (OLA) is a well-known food additive that is highly phototoxic, mutagenic, genotoxic, and carcinogenic. Tetracycline (TC) is one of the most widely used antibiotics in the world and has serious side effects on human health and potential negative effects on the environment when it accumulates in water systems. Thus, effective removal of organic pollutants from contaminated water is of great importance. The current priority is to develop novel adsorbent materials with high adsorption capacities and removal efficiencies to realize effective control of these environmental pollutants. Various researchers have examined the potential of CNTs for the removal of different organic pollutants from water and Table 2 summarizes the removal of organic pollutants using various types of carbon nanotubes.

Even through carbon nanotubes have many significant advantages, but their use on an industrial scale for practical applications is not expected in the midterm because of their high production costs [91]. Point-of-use applications that require small quantities of CNTs are more competitive; for example, for the elimination of heavily degradable contaminants such as many antibiotics and pharmaceuticals [92–94]. Therefore, more research is needed to come up with the practical and economical solutions for using CNTs in water treatment.

2.1.2. Graphene based materials

Research has also been focused on another allotropy of carbon, which is graphene. From the past decade, there is a huge growth in the use of graphene and graphene based materials for environmental remediation, due their unique properties which helps to new possibilities to improve the performance of numerous environmental processes. There is a choice of whether to use graphene

Table 2
Removal of organic pollutants using various types of carbon nanotubes.

S. No.	Type of CNTs	Organic pollutants	Adsorption capacity (mg/g)	Refs.
1.	Alkali-activated MWCNTs	Methylene blue	399	[75]
2.	Untreated MWCNTs	Methylene blue	59.7	[76]
3.	Untreated SWCNTs	Reactive red 120 (RR -120)	426.49	[62]
4.	Oxidized SWCNTS	Basic red 46 (BR 46)	49.45	[77]
5.	Untreated MWCNTs	Tetracycline (TC)	269.54	[78]
6.	MWCNTs	Olaquindox	99.7%	[79]
7.	SWCNTs	4-Chloro-2-nitrophenol	1.44	[80]
8.	MWCNTs	4-Chloro-2-nitrophenol	4.42	[80]
9.	Untreated SWCNTs	Dissolved organic matter (DOM)	26.1–20.8	[81]
10.	KOH activated MWCNTs	Toluene, ethylbenzene, m-xylene	87.12, 322.05, 247.83	[82]
11.	MWCNTs	Methyl orange	52.86	[83]
12.	Chitosan/Fe_2O_3/MWCNTs	Methyl orange	66.90	[84]
13.	Calcium alginate/MWCNTs	Methyl orange	12.5	[84]
14.	MWCNTs	Tetracycline	192.7	[85]
15.	CNTs-C@Fe-chitosan composite	Tetracycline	104	[86]
16.	Single, double and multiwalled carbon nanotubes	Oxytetracycline	554, 507, 391	[87]
17.	Single, double and multiwalled carbon nanotubes	Ciprofloxacin	933.8, 901.2, 651.4	[87]
18.	MWCNTs/$CoFe_2O_4$	Sulfamethoxazole	6.98	[88]
19.	Pristine and hydroxylated MWCNTs	Sulfamethazine	24.78, 13.31	[89]
20.	Carboxylated multiwalled carbon nanotubes	Norfloxacin	90.3	[90]

as a carbon-based nanocomposite will be determined by the cost, process ability, and environmental implications of each material. In this regard, environmental applications based on GO offer more realistic possibilities compared to pristine graphene due to GO's lower production costs. In addition to economic considerations, environmental implications of graphene-based materials will represent an important factor in the development of graphene-based technologies. Graphene is a substitute for CNT and an ideal material for water treatment. Compared to CNTs, the utilization of graphene-based materials as adsorbents may offer several advantages. First, single-layered graphene materials possess two basal planes available for pollutant adsorption [47,95–97]. In contrast, the inner walls in CNTs are not accessible by the adsorbates [95]. Second, graphene oxide (GO) and reduced graphene oxide (rGO) can be easily synthesized through chemical exfoliation of graphite, without using complex apparatus or metallic catalysts. The resulting graphene material is free of catalyst residues, and no further purification steps are needed. In the specific case of GO, the as-prepared material already possesses a large number of oxygen-containing functional groups and no additional acid treatments are required to impart a hydrophilic character and reactivity to GO [98]. This is a significant advantage, since those functional groups are likely responsible for the adsorption of metal ions by GO sheets.

Graphene based materials serve as efficient adsorbent, due to their large specific surface area and electron rich environment. Due to the strong functional groups on graphene oxide (GO) surface, GO will be a potential adsorbent for metal ion complexation through both electrostatic and coordinate approaches. A variety of studies have described the application of graphene based materials as adsorbents for the removal of inorganic species from aqueous solutions [98]. Most of these studies have employed GO as a model adsorbent for remediation of metal ions in water [99–101]. GO is preferable to pristine graphene for metal ion adsorption due to GO's high content of oxygen groups available to interact with metal ions. The importance of these oxygen-containing functional groups was demonstrated by comparing the Pb(II) adsorption performance of pristine and oxidized graphene sheets [102]. GO and graphene nanosheets (GNs) can also be incorporated with metal oxides to form composite materials. A composite with GO and metal oxide usually has specific features and has been used as effective adsorbents for the removal of different pollutants. Flower-like TiO_2 on GO hybrid (GO–TiO_2) has been used for the removal of Zn^{2+}, Cd^{2+} and Pb^{2+} ions from water [103]. The adsorption capacities of GO–TiO_2 hybrid reached 88.9 mg/g for Zn^{2+}, 72.8 mg/g for Cd^{2+}, and 65.6 mg/g for Pb^{2+}, respectively, at pH 5.6, which are higher than either GO or TiO_2 as shown in Table 3.

Pristine graphene was first prepared through a vacuum-promoted low-temperature exfoliation and submitted to heat treatments at 500 and 700 °C (GNS500 and GNS700) to introduce oxygen functional groups. GNS500 and GNS700 revealed a higher adsorption capacity for Pb(II) compared to pristine graphene, which underscores the importance of carboxyl groups in the adsorption mechanism of Pb(II) [102]. Besides metals removal, graphene based adsorbents have also been used for the removal of various organic pollutants from water and Table 4 summarizes the removal of organic pollutants using graphene based adsorbents.

The fate, transformation, and toxicological impacts of graphene based materials in the environment have been extensively reviewed in previous literature [134–136]. However, the importance of carefully evaluating the environmental implications of graphene based materials must be emphasized. Detailed ecotoxicological assessments and life-cycle analyses still need to be performed, in order to identify the forms of graphene-based nanomaterials that will allow us to utilize the properties of graphene, while minimizing the associated health and environmental impacts. Until these economic and environmental considerations are known and better understood, it would be hard to determine the most promising areas of research for graphene-based materials. One of the most important challenges will be to reduce GO successfully to a pristine graphene material in order to restore its exceptional electronic and mechanical properties. Reduction of GO for the production of graphene certainly appears a most promising approach to produce low cost graphene on a large scale.

2.2. Metal oxide based nanomaterials

2.2.1. Nano metal oxides

Among the available adsorbents, nanosized metal oxides (NMOs), including nanosized ferric oxides, manganese oxides, aluminum oxides, titanium oxides, magnesium oxides and cerium oxides, are classified as the promising ones for removal of pollutants from aqueous systems [137–139]. This is partly because of their large surface areas and high activities caused by the size quantization effect [140,141]. Recent studies suggested that many NMOs exhibit favorable sorption to heavy metals in terms of high capacity and selectivity, which would result in high removal of toxic metals to meet increasingly strict regulations [142]. However, as the size of the metal oxides reduces from micrometer to nanometer levels, the increased surface energy inevitably leads to their poor stability. Consequently, NMOs are prone to agglomeration due to van der Waals forces or other interactions [143], and the high capacity and selectivity of NMOs would be greatly decreased or even lost. Moreover, NMOs are unusable in fixed beds

Table 3
Various graphene based nanocomposites for the removal of some heavy metal ions.

S. No	Adsorbent	Adsorbate	Adsorption capacity (mg/g)	Refs.
1.	GO/Fe_3O_4	Cu(II)	18.3	[104]
2.	GO/silica/Fe_3O_4	Pb and Cd (II)	333.3 and 166.7	[105]
3.	GO/Fe_3O_4/sulfanilic acid	Cd (II)	55.4	[106]
4.	GO-$MnFe_2O_4$	Pb(II)	673	[107]
5.	rGo/$COFe_2O_4$	Pb(II)	299.4	[108]
6.	GO/Mn-doped Fe(III)oxide	Cd and Cu(II)	87.2 and 129.7	[109]
7.	GO/Fe_3O_4/sulfanilic acid	Cu(II)	50.7 and 56.8	[110]
8.	GO/Fe_3O_4	Cu, Pb and Cd	23.1, 38.5 and 4.4	[111]
9.	Graphene Oxide (GO)	Pb(II)	35.6	[103]
10.	TiO_2/GO	Pb(II)	65.6	[112]
11.	GO-EDTA	Pb(II)	479	[112]
12.	Graphene nanosheets (GNs)	Pb(II)	22.4	[102]
13.	GNs-500	Pb(II)	35.2	[102]
14.	SiO_2–GNs	Pb(II)	113.6	[113]
15.	MnO_2/GNs	Hg (II)	10.8	[114]

Table 4
Adsorption of organic pollutants using graphene based materials.

S. No.	Adsorbent	Organic pollutants	Adsorption capacity (mg/g)	Refs.
1.	Polyethersulfone/GO	MB	62.50	[115]
2.	Fe_3O_4/GO hybrids	MB, NR	167.2, 171.3	[116]
3.	Reduced GO–MFe_2O_4 hybrids	RhB, MB	92% and 100%	[117]
4.	GO sponge	MB, MV	397, 467	[118]
5.	Reduced GO/ZnO nanohybrids	RhB, MB	–	[119–121]
6.	Reduced GO/CdS hybrids	MB	94%	[122]
7.	Reduced GO–TiO_2	MO	–	[123]
8.	Fe_3O_4–GNs	MB,CR	45.3, 33.7	[124]
9.	GO	MB	351	[125]
10.	GNs	MB	154–204	[126]
11.	GO	Tetracycline	313.48	[127]
12.	GO	Oxytetracycline	212.31	[127]
13.	GO	Doxycycline	398.40	[127]
14.	F–GO with MNPs	Oxytetracycline	45.0	[128]
15.	F–GO with MNPs	Tetracycline	39.1	[128]
16.	F–GO with MNPs	Chlortetracycline	42.6	[128]
17.	F–GO with MNPs	Doxycycline	35.5	[128]
18.	TiO_2-graphene sponge	Tetracycline	1805	[129]
19.	GO	Tetracycline	381.77	[130]
20.	Single layer GO	Ciprofloxacin	379	[131]
21.	KOH-activated graphene	Ciprofloxacin	194.6	[132]
22.	Porous graphene hydrogel	Ciprofloxacin	235.6	[133]

or any other flow through systems because of the excessive pressure drops (or the difficult separation from aqueous systems) and poor mechanical strength. To improve the applicability of NMOs in real wastewater treatment, these were impregnated into porous supports of large size to obtain composite adsorbents [144]. The widely used porous supports include activated carbon, natural materials, synthetic polymeric hosts, etc. Besides traditional NMOs, magnetic NMOs attract increasing attentions as they can be easily separated from water under a magnetic field [145]. Also, magnetic NMOs-based composite adsorbents allowed easy isolation from aqueous solutions for recycling or regeneration [146]. Such facile separation is essential to improve the operation efficiency and reduce the cost during water/wastewater treatment.

Since there are so many types of NMOs employed for heavy metals removal, comparison of their capacity is necessary. However, the experimental conditions in the related references varied greatly and thus, a direct comparison of the reported data seems a little meaningless. For example, due to the different synthetic methods of a given NMO, it is difficult to keep constant its size and surface chemistry. In addition, the operating conditions, like the solution chemistry (pH, ionic strength and ion types), temperature, experimental form (batch or column runs) are quite different from each other. Here, a simple comparison on some typical NMOs for metals removal has been made (Table 5).

2.2.2. Nano metal oxides supports

Nano metal oxides (NMOs) show an effective and specific adsorption towards various aquatic pollutants. Nevertheless, they are usually present as fine or ultrafine particles, which often lead to problems such as activity loss due to agglomeration, difficult separation, and excessive pressure drops when applied in flow-through systems [154]. An effective approach to overcome these technical bottlenecks is to fabricate hybrid adsorbents by impregnating or coating NMOs particles into/onto porous supports of larger size [155–158]. The widely used supports include natural hosts such as bentonite [159,160], sand [161,162], and metallic oxide materials such as Al_2O_3 membrane [163], porous manganese oxide complex [164], and synthetic polymer hosts such as cross-linked ion-exchange resins [165–167]. Some host-supported NMOs for heavy metals removal are summarized in Table 6.

Table 5
Adsorption capacities of nano metal oxides for metals removal.

S. No	Adsorbent	Adsorbate	Temp. (°C)	Adsorption capacity (mg/g)	Refs.
1.	Goethite (α-FeOOH)	Cu(II)	25	149.25	[147]
2.	Hematite (α-Fe_2O_3)	Cu(II)	25	84.46	[148]
3.	γ-Fe_2O_3	Cu(II)	25C	26.8	[149]
4.	ZnO	Pb(II)	28C	6.7	[150]
5.	CeO_2	Pb(II)	28C	9.2	[151]
6.	TiO_2	Pb(II)	25C	401.14	[152]
7.	Modified Al_2O_3	Pb(II) and Cd(II)	25C	100 and 83.33	[153]

Table 6
Nano metal oxides support materials for the removal of heavy metal ions.

S. No.	Metal oxide	Support material	Adsorbents	Adsorption capacity (mg/g)	Refs.
1.	Iron oxide	Treated municipal sewage sludge	Pb(II) & Cd(II)	42.4 and 14.7	[168]
2.	Fe_3O_4	Cyclodextrin	Cu(II)	47.2	[169]
3.	Fe_2O_3	Sepiolite	Ni(II)	18.30	[170]
4.	Manganese oxide	Diatomite	Pb(II) & Cd(II)	99.0 and 27.86	[171]
5.	ZnO	Activated carbon	Pb(II)	100% removal	[172]
6.	Nanosize calcium titanate	Aluminium oxide	Pb(II) and Cd(II)	124 and 8.58	[173]
7.	Goethite	Sand	Pb(II) and Cd(II)	702 and 704 µg/g	[174]

To date, metal oxides are widely explored as highly efficient adsorbents for pollutants removal from water/wastewater. They exhibit various advantages such as fast kinetics, high adsorption capacity, and preferable sorption towards pollutants in water and wastewater. Nevertheless, to further promote the practical application of metal oxides in abatement of various pollutants, there still exist some technical bottlenecks to be solved. For instance, when applied in aqueous solution, metal oxides tend to aggregate into large-size particles and their capacity loss seems inevitable. In addition, the way to efficiently separate the exhausted metal oxides from water/wastewater still remains an interesting but a challenging task. As for column operation, the excessive pressure drop caused by metal oxides should also be considered.

Fortunately, fabrication of new metal oxides based composite adsorbents seems to be an effective approach to respond to all the above technical problems. However, it is still in the infant stage, and various issues need to be solved concerning the development of more facile processes to obtain the composite adsorbents, and the answer is to interplay between the hosts and the supported metal oxides, the long-term performance of the composite adsorbents, as well as their field application in heavy metal contaminated water treatment.

Recently, magnetic adsorbents have attracted intensive interest in water treatment due to its easy separation and collection using a magnet. Incorporation of magnetic particles with GO or GNs offer an effective approach to overcome the separation problems associated with graphene. At the same time, loading of the magnetite nanoparticles can avoid or decrease the possibility of serious agglomeration and restacking of the graphene sheets, and consequently provide a higher available surface area and enhancement of adsorption capacity [175]. Liu et al. [176] have reported a mag-

netite Fe_3O_4/GO composite (M/GO) for the removal of Co^{2+} from aqueous solutions and investigated adsorption kinetics, equilibrium and thermodynamics. M/GO was found to have a higher adsorption than that of Fe_3O_4 and could be separated and recovered by magnetic separation after adsorption. Santhosh et al. have reported a G-Fe_3O_4 nanocomposite for the removal of Pb^{2+} from aqueous solution and also investigated its adsorption and as antibacterial activity [177].

$MnFe_2O_4$-G ferrites have been used for the effective removal of Pb and Cd ions. Sorption of Pb and Cd ions onto $MnFe_2O_4$-G surface followed pseudo second order kinetic model and the monolayer adsorption capacity of Pb and Cd on $MnFe_2O_4$-G was found to be 100 and 76.90 mg/g at pH 5 and 7 respectively. Effect of $MnFe_2O_4$-G on bacterial model *E. coli* was also investigated with 82% loss of viability after 2 h of treatment with 100 mg/L $MnFe_2O_4$-G (Fig. 2) [178].

$CoFe_2O_4$-G and $NiFe_2O_4$-G have been tested for the heavy metal ions removal and results showed that the adsorption capacity for Pb and Cd ions. The maximum adsorption for Pb ions was found to be 142.8 and 111.1 mg/g at pH 5, 310 K for $CoFe_2O_4$-G & $NiFe_2O_4$-G, whereas for Cd ions, it was found to be 105.26 and 74.62 mg/g at pH 7 and 310 K respectively. Thermodynamic properties signifies that the adsorption reaction was spontaneous and exothermic [179].

Synthesis of magnetite nanoparticles (MNPs) using low cost approach has also been conducted [180]. Iron ore tailings (IOT) as the primary source of MNPs was taken into consideration during the study. Methylene blue (MB) and Congo red (CR) dyes were taken as the model pollutants. Complete recovery of iron from IOT was made with HCl. Finally, ferric (hydro) oxide (FHO) (primarily constituting of goethite) was yielded after treatment
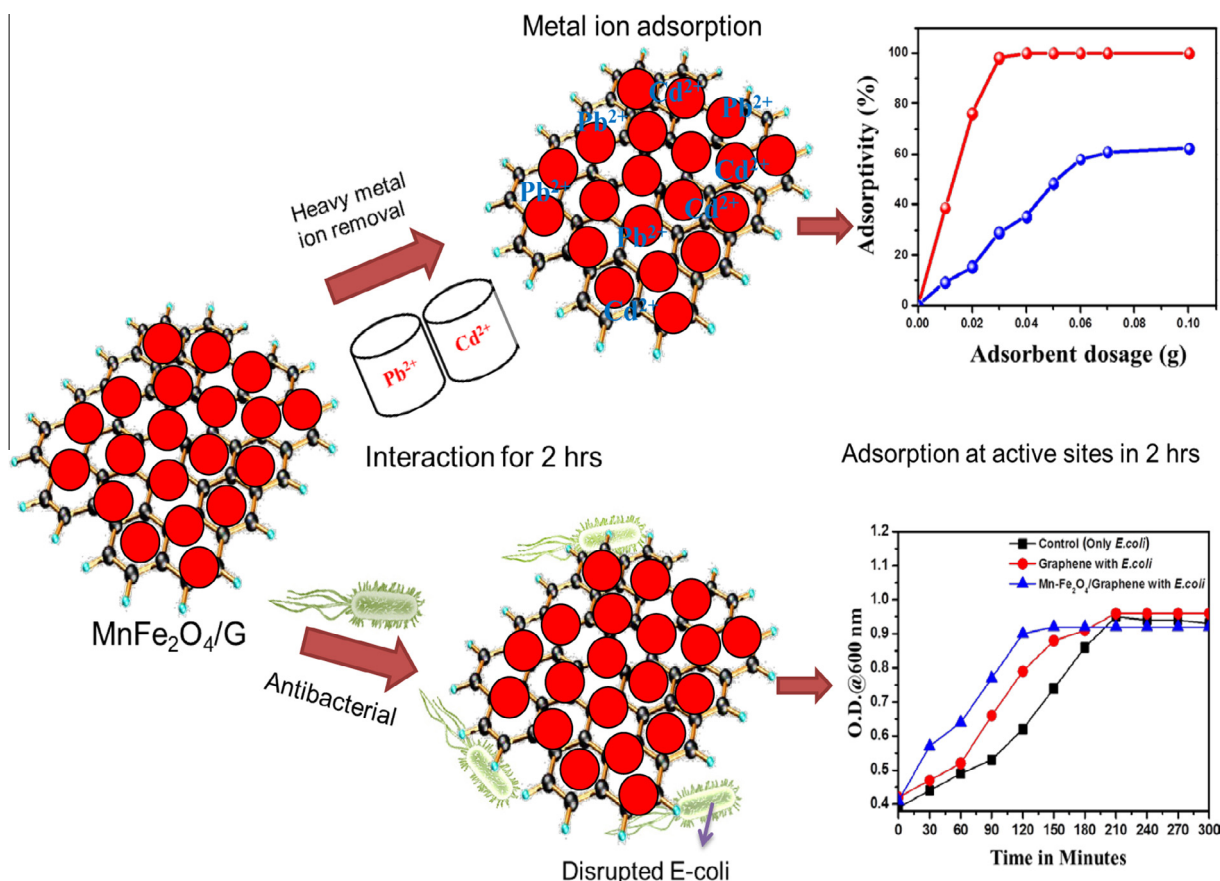

Fig. 2. Schematic diagram showing the adsorption of heavy metal ions and antibacterial activity on $MnFe_2O_4$-G. (Reproduced from Ref. [178] by permission of Elsevier.)

with concentrated ammonia. The adsorbent pH was raised with NaOH and stabilized using sodium dodecyl sulphonate (SDS). The chemical analysis of synthesized MNPs showed that total iron content was close to theoretical value (72.36%). The pHpzc of MNPs was found to be 7.1. The results of adsorption studies of MB and CR dyes exhibited that the kinetics of the process was rapid showing that the adsorption occurred only on the surface of MNPs. The behavior of MNPs towards the varying pH was explained on the basis of pHpzc (pHpzc: ∼7.1) and the adsorption of cationic MB was found to be higher above pHpzc and anionic CR adsorption was higher in the lower pH range. The optimized pH for MB and CR dyes adsorption was found to be ∼9.2 and ∼6.2, respectively. The aggregation of MNPs on the increase of MNPs dose was noticed leading to a non-linear adsorption of dyes. Increase in dyes concentrations lead to an increase in dyes uptake by MNPs but the percentage adsorption decreased. The monolayer adsorption capacities of MNPs (70.4 and 172.4 mg/g for MB and CR, respectively, were obtained. Desorption studies of MB and CR dyes were also performed and 95% CR was found to desorb at pH > 8.0. However, MB desorption was more effective (85% MB desorption) when methanolic solution of acetic acid (4% (v/v) acetic acid in methanol) was used as an eluent.

In an attempt to modify the iron oxide nanoparticles for rendering them effective for dye removal, Inbaraj and Chen [181] synthesized poly(γ-glutamic acid) (PGA) coated iron oxide nanoparticles. PGA coating was found to improve the stability of the MNPs that was confirmed by the leaching experiments in different aqueous matrices (deionized water, tap water, river water, acidic solutions, basic solutions). The MB dye experimental isotherm data fitted well to the Redlich–Peterson and Langmuir models. The maximum adsorption capacity of MB dye onto PGA-MNPs obtained from Langmuir model was found to be 78.67 mg/g. The adsorption kinetics of MB onto synthesized nanomaterials was fast (equilibrium was achieved in 5 min). In the presence of coexisting ions, MB adsorption was lowered. A declining trend in presence of CaCl2 was more significant than in presence of NaCl due to the valence effect. Acidic pH (1.0–3.0) was not favorable for the adsorption of MB dye onto PGA-MNPs due to the competition between dye cations and hydrogen ions in the solution for the α-carboxylate anions present on the surface of the adsorbent. Ion exchange mechanism that dominated at higher pH favored the MB adsorption onto PGA-MNPs. On the other hand, desorption was favorable in acidic media (ionized water). Salih et al. [182] investigated the fate and transport of Fe2O3 NPs in a granular activated carbon (GAC) adsorber bed and its impact on trichloroethylene (TCE) adsorption. The presence of Fe2O3 NPs enhanced the TCE removal

(70%) from aqueous phase as compared kinetics onto GAC alone. But, desorption was similarly fast due to the absence of a suitable pore size distribution for permanent adsorption of TCE. The characterization results revealed that only 3% of Fe2O3 NP total surface area was microporous resulting in their easy desorption into bulk solution. It was concluded from the values obtained from the kinetic models that batch systems might not be optimal to study TCE adsorption. The column breakthrough studies were also undertaken in which it was observed that TCE breakthrough occurred in a shorter time in presence of Fe2O3 NPs than in their absence. This was attributed to the attachment of Fe2O3 onto GAC. Also, the impact of Fe2O3 NPs on TCE breakthrough was found to be concentration dependent. Besides metals removal, nano metal oxides based adsorbents have also been used for the removal of various organic pollutants from water and Table 7 summarizes the removal of organic pollutants using nano metal oxides based adsorbents.

Although, the use of metal oxide nanoparticles in various applications including water treatment is increasing tremendously, but still there are some adverse effects of using metal oxide nanoparticles on the health of living organisms [198]. There are various studies on the toxicity of metal oxide nanoparticles and there is also an increase in the cytotoxic potential of these metal oxide nanoparticles [199]. Hence there is a challenging task of preparing eco-friendly metal oxide nanoparticles with better efficiency and minimum negative effects to the environment.

2.3. Miscellaneous nanoadsorbents

Besides the above categorized nanoadsorbents, there are some other nanoadsorbents which have been prepared and applied in water treatment by different researchers. A brief discussion is presented here. Chitosan–Fe(0) nanoparticles (chitosan–Fe(0)) were prepared using biodegradable chitosan as a stabilizer and batch experiments were conducted to evaluate the influences of initial Cr(VI) concentration and other factors on Cr(VI) reduction on the surface of the chitosan–Fe(0) [200]. The authors suggested that the overall disappearance of Cr(VI) might include both physical adsorption of Cr(VI) onto the chitosan–Fe(0) surface and subsequent reduction of Cr(VI) to Cr(III). Characterization with high-resolution X-ray photoelectron spectroscopy revealed that after the reaction, relative to Cr(VI) and Fe(0), Cr(III) and Fe(III) were the predominant species on the surface of chitosan–Fe(0). Chitosan also inhibited the formation of Fe(III)–Cr(III) precipitation due to its high efficiency in chelating the Fe(III) ions. The adsorption of eosin Y, as a model anionic dye, from aqueous solution using

Table 7
Removal of organic pollutants using nano metal oxides.

S. No	Adsorbents	Organic pollutants	Adsorption capacity (mg/g)	Refs.
1.	SiO2/Fe3O4	MO	53.19	[183]
2.	γ-Fe2O3/SiO2/chitosan composite	MO	34.29	[184]
3.	γ-Fe2O3 crosslinked chitosan composite	MO	29.46	[185]
4.	Magnetic nanopowder	Phenol	13.5	[186]
5.	γ-Fe2O3/2C nanocomposite	Phenol	42.34	[187]
6.	γ-Fe2O3/2C nanocomposite	MO	72.68	[187]
7.	γ-Fe2O3	Acridine orange	59	[188]
8.	Polyacrylic acid-Fe3O4	MB, Crystal violet	199,116	[189,190]
9.	Fe3O4-CTAB	Acid red 27	1.05	[191]
10.	CTAB-Fe3O4/SiO2	Phenolic compounds	–	[192]
11.	Chitosan-Fe3O4	Acid orange 12 acid green 25	1.883,1.471	[193]
12.	Fe3O4@SiO2/SiCRG	Metoprolol (MTP)	447	[194]
13.	SiO2/SiCRG	Metoprolol (MTP)	393	[194]
14.	Silica gel	Metoprolol (MTP)	68.4	[195]
15.	α-Fe2O3	Congo red	413.22	[196]
16.	Qur-Fe2O3	Congo red	619.51	[196]
17.	Fe3O4 MNPs	Crystal violet	166.67	[197]

chitosan nanoparticles, prepared by the ionic gelation between chitosan and tripolyphosphate, was examined by Du et al. [201]. The adsorption capacity was found to be 3.33 g/g. The adsorption process was endothermic in nature with an enthalpy change (ΔH) of 16.7 kJ/mol at 20–50 °C. The optimum pH value for eosin Y removal was found to be 2–6. The dye was desorbed from the chitosan nanoparticles by increasing the pH of the solution. The desorption percentage was about 60% within 60 min at pH 11.0, whereas 98.5% of the dye could be eluted at pH 12 in 150 min. The potential of nanochitosan to remove acid dyes from aqueous solution has also been explored by the researchers [202]. The monolayer adsorption capacities were determined to be 1.77, 4.33, 1.37 and 2.13 mmol/g for acid orange 10, acid orange 12, acid red 18 and acid red 73 dyes, respectively. The differences in capacities might be due to the differences in the size of dye molecules and the number of sulfonate groups on each dye molecule. The results have demonstrated that monovalent and smaller dye molecular sizes have superior capacities due to the increase in dye/chitosan surface ratio in the system and deeper penetration of dye molecules into the internal pore structure of nanochitosan. The mechanism of the adsorption process of acid dye on nanochitosan was proposed to be the ionic interactions of the colored dye ions with the amino groups on the chitosan. By encapsulating zirconium phosphate (ZrP) nanoparticles into three macroporous polystyrene resins with various surface groups, i.e., $-CH_2Cl$, $-SO_3$ and $-CH_2N+(CH_3)_3$ three nanocomposite adsorbents (denoted as ZrP–Cl, ZrP–S, and ZrP–N) were fabricated, respectively for lead removal from water [203]. Effect of functional groups on nano-ZrP dispersion and effect of ZrP immobilization on the mechanical strength of the resulting nanocomposites were investigated. The presence of the charged functional groups ($-SO_3$ and $-CH_2N$ $+(CH_3)_3$) were more favorable than the neutral $-CH_2Cl$ group to improve nano-ZrP dispersion (i.e., to achieve smaller ZrP nanoparticles). ZrP–N and ZrP–S had higher capacity than ZrP–Cl for lead removal. As compared to ZrP–N, ZrP–S exhibited higher preference towards lead ions at high calcium levels as a result of the potential Donnan membrane effect. On the other hand, nano-ZrP immobilization would simultaneously reinforce both the compressive strength and the wear performance of the resulting nanocomposites with the ZrP loadings up to 5 wt%.

The organic-inorganic hybrid of poly(acrylic acid-acrylonitrile)/attapulgite, P(A-N)/AT nanocomposites, were prepared by using in situ polymerization and composition of acrylic acid (AA) and acrylonitrile (AN) onto modified attapulgite (AT) nanoparticles [204]. The resulting P(A-N)/AT nanocomposites were transformed into novel nano-adsorbent of poly(acrylic acid-acryloamidoxime)/attapulgite by further functionalization, i.e., P(A-O)/AT nano-adsorbent. The adsorption properties of P(A-O)/AT toward metal ions were determined, and the results indicated that the adsorbents with nanocomposite structure held a good of selectivity to Pb(II) among numerous metal ions. The maximum removal capacity of Pb(II) was up to 109.9 mg/g and it was notable to see that the adsorption removal of P(A-O)/AT nano-adsorbent for Pb(II) could achieve more than 96.6% when the initial concentration of Pb(II) was 120.0 mg/L. Besides the above mentioned nanoadsorbents, several other materials have also been examined as nano-adsorbents for the removal of different aquatic pollutants [27,205–222].

Raveendra et al. [223] have synthesized nanocrystalline *meta*-zinc titanate (ZnTiO$_3$) ceramic using a self-propagating solution combustion synthesis (SCS) using urea as fuel. The preparation and characterization of ilmenite type nanocrystalline ZnTiO$_3$ ceramic were discussed in detail and studied its effectiveness in the adsorption of hazardous malachite green (MG) dye. Mechanism of adsorption of MG onto the nanocrystalline ZnTiO$_3$ ceramic was explained on the basis of pH effect. Under acidic conditions, it

was difficult for cationic MG dye to adsorb onto the nanocrystalline ZnTiO$_3$ surface. This is because, as initial pH of dye solution decreased, the number of negatively charged adsorbent sites decreased and positively charged sites increased which did not favor the adsorption since the MG is a cationic dye resulting in electrostatic repulsion. This decrease in the adsorption at lower pH was also due to the fact that the presence of excess H$^+$ released from the MG dye at acidic condition which opposed with dye cations for the adsorption. In turn, at higher pH, the negatively charged sites on adsorbent molecule increased which attracted the positively charged sites of cationic MG dye resulting in higher adsorption. The results showed that the parameters such as effect of pH and contact time played a very important role on the adsorption. Adsorption kinetics results show that adsorption of MG over ZnTiO$_3$ followed first order kinetics.

Taghizadeh et al. [224] have synthesized nickel nanoparticles (Ni–NP) and zinc selenide nanoparticles (Zn–Se–NP) which were loaded on activated carbon and used for the removal of Arsenazo (III) dye from aqueous medium. The results show that Langmuir plot for Arsenazo (III) adsorption on both adsorbents is linear over the whole concentration range studies and the correlation coefficients were extremely high ($R^2 > 0.99$). Heat of adsorption and the adsorbent–adsorbate interaction were studied by Tempkin and Pyzhev models. Adsorption equilibrium data were also fitted with Dubinin and Radushkevich isotherm models. From the correlation coefficient it was concluded that the adsorption was not fitted well with Dubinin and Radushkevich isotherm model. The high Arsenazo (III) removal using both adsorbents showed their applicability to remove the dye in short equilibrium time (less than 25 min). Adsorption kinetics was found to follow a second-order rate expression and equilibrium adsorption data for both adsorbents were best represented by the Langmuir isotherms. Higher inhibition field of nickel nanoparticle (120–205 Oe) in comparison to respective value for bulk nickel may be attributed to decrease in the size of produced nickel and formation of nanoparticle. The Ni–NP–AC was efficient for quantitative removal of Arsenazo (III) (98% within 20 min). It was found that the dye removal efficiency of Ni–NP– AC was superior than that of Zn–Se–NP–AC. The maximum adsorption capacity of Ni–NP–AC and Zn–Se–NP–AC was found as 168 and 162.74 mg/g, respectively.

2.4. Silsesquioxane based materials

A silsesquioxane is an organosilicon compound with the chemical formula [RSiO$_{3/2}$]$_n$ (R = H, alkyl, aryl or alkoxyl) [225]. Silsesquioxanes are members of polyoctahedral silsesquioxanes ("POSS"), which have attracted attention as precursors to ceramic materials and nanocomposites. The potential applications of silsesquioxane based materials lie in the fields of catalysis [226,227], separation and storage [228,229], opto-electronics [230] and environmental field [231–233]. These materials are extensively used for the synthesis of nano structured hybrid polymer materials, having nanometer sized inorganic cores surrounded with organic functional groups [225,234–236].

There are diverse POSS based nanocomposites which have been developed [237,238], and generally, there are mainly three approaches for integrating POSS into nanocomposites: first is the core as a POSS function and the microinitiator to initiate polymerization from the surface of the POSS, giving a star-like macromolecules; second is multi-functional POSS compounds which can function as nano fillers or monomers to polymerize with organic monomers or polymers, forming crosslinked nanocomposites and the third is monofunctional POSS compounds as tethering macromolecules to graft onto a polymer backbone, forming polymers with pedant POSS cages. Star-like nanocomposites with POSS as the core are generally prepared using functional POSS as the

micro-initiator. For example, by reacting octa(aminophenyl) silsesquioxane (OAPS) with 2-bromo-isobutyryl bromide, octa-butyrylbromide POSS can be obtained and it can subsequently initiate atom transfer radical polymerization (ATRP) of 2,2,3,4,4,4-hexafluorobutyl methacrylate (HFBMA) or methyl methacrylate (MMA) [239]. Due to the incorporation of a thermally stable inorganic Si–O core, the star-like POSS-g-HFBMA exhibits improved thermal properties.

Shena and Liu [240] have selected the triphenylphosphine (TPP) and triphenylphosphine oxide (TPPO) materials to react with cubic octavinylsilsesquioxane (OVS) for preparing the two novel parallel series of hybrid phosphorus-containing porous polymers (denoted as HP-TPPs and HP-TPPOs) via the Friedel–Crafts reaction, respectively. These hybrid porous polymers possessed high surface areas, unique bimodal pores with uniform micropores and mesopores centered at 1.5 nm and 3.7 nm, respectively, and an excellent size-selective adsorption for dyes. They displayed an outstanding adsorption ability for Rhodamine B (RhB) with maximum adsorption capacities of 828.6 mg/g, and could rapidly remove more than 90% RhB within 3 min when the initial concentration of the RhB solution was 50 ppm.

Liu et al. reported the removal of Pb^{2+} ions from aqueous solutions by using synthetic polymer P(AO/AN/MA) which achieved an adsorption capacity of 4.28 mmol/g at 25 °C [241]. Polymers which could selectively adsorb metal ions should consist of two monomer groups, each having a different role. One functional group forms a complex with the target and the other allows the polymers to stretch and shrink reversibly in response to environmental change. Generally, amidoxime (AO) and carboxylic groups (AA) were chosen as the functional groups [242–244].

Based on the discussion above, it can be concluded that these materials are very promising to be industrialized and be of great use in the field of wastewater treatment. A future direction for the development of POSS-containing materials is also proposed for applications in organic photovoltaic and other high-performance materials.

3. Nanomaterials as photocatalysts

During recent decades, the photocatalytic degradation of various toxic organic compounds has been proposed as a viable process to detoxify water. Much attention has been paid to the photocatalytic degradation of dyes with TiO_2 particles under UV or visible light since conventional biological treatment processes are not effective in degrading these pollutants in wastewater [245,246]. There are various proposed mechanisms for the degradation of dyes using the photocatalyst materials. One mechanism suggests that the oxidation of organic compounds is first initiated by the free radicals, which are mainly induced by the electron–hole (e^-/h^+) pairs at the photocatalyst surface [247]. Another mechanism states that the organic compound is firstly adsorbed on the photocatalyst surface and then reacts with excited superficial e^-/ h^+ pairs or OH radical to form the final products [248]. A variety of reaction mechanisms depend on both surface adsorbed and solution phase species, resulting in different kinetics of photodegradation. Adsorption of the organic pollutants is generally considered to be an important parameter in determining degradation rates of photo catalytic oxidation [249].

Semiconductor materials have shown good photocatalytic activity on removing various organic pollutants. However, commercial visible light photocatalysts show some disadvantages, either they are unstable or inefficient upon the illumination of light. Recently, group II–VI semiconductors with energy gaps covering the visible spectral range have been recognized as compatible candidates for photocatalysts. Many studies have been reported exploring the novel materials, which can act as highly efficient material under visible light, and act as an active photocatalyst for the degradation of different organic pollutants with high efficiency and high stability [250].

Shen et al. [251] prepared ZnCdS nanoparticles decorated on a 2D platform of reduced graphene oxide (rGO) sheets by a one-pot ionic-liquid-assisted hydrothermal process towards photocatalytic activities toward the photo-degradation of organic dyes (Fig. 3).

Generally, three factors are crucial for the photocatalytic activities of the composite, namely, the adsorption of contaminant molecules, light irradiation absorption, and charge transportation and separation [252]. The photocatalytic degradation of organic pollutants using TiO_2 as photocatalyst has been widely studied. However, TiO_2 is only activated under UV irradiation, which greatly limits the efficient utilization of solar energy. In the case of ZnCdS, its valence band energy is about 1.0 eV more negative than that in the case of TiO_2. It causes the narrowing of bandgap energy and response to visible light [253]. On the other hand, because of the unique properties of graphene, it cannot only improve the separation and transport of photocarriers, but also
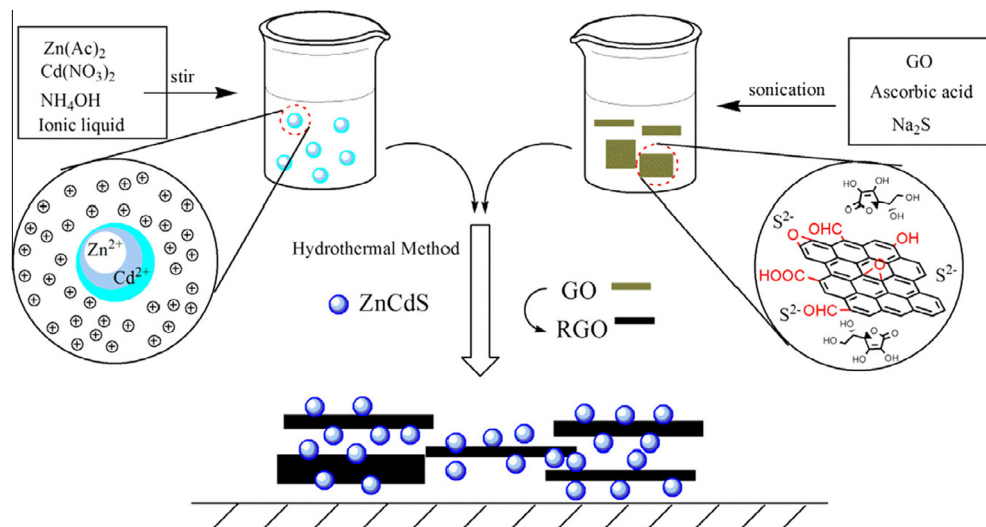

Fig. 3. Experimental procedure used to prepare rGO–ZnCdS. (Reproduced from Ref. [251] by permission of Elsevier.)

might cause a higher conduction band position with a stronger reductive power. Photo catalytic activity was evaluated by the degradation of methyl orange and RhB in aqueous solution under visible light with different weight loadings of rGO into the ZnCdS [251]. From Fig. 4, it can be found that the degradation of methyl orange over the as-prepared catalyst within a 24 h reaction time decreased in the order of rGO–ZnCdS-3 > rGO–ZnCdS-2 > rGO–ZnCdS-4 > rGO–ZnCdS-1 > ZnCdS (Fig. 4a). Similar results were also observed for the degradation of RhB under visible light irradiation (Fig. 4b). It seems that with the increase of the content of rGO, the photoactivity with respect to degradation of dyes is enhanced gradually at first but decreased with higher loading ratio. Excessive addition of black color rGO will lower the light intensity through the depth of the reaction solution, thus decreasing its photoactivity.

It was found that there were at least three reasons for the remarkable photocatalytic activity of rGO–ZnCdS for the bleaching of organic dye under visible-light irradiation. First, rGO–ZnCdS has enhanced adsorption of organic dyes molecules; second, rGO–ZnCdS has an obviously extended photo-responsive range; finally, the formed rGO–ZnCdS hetero system has a synergetic effect on its photoactivity.

Xiong et al. [254] synthesized graphene–gold nanocomposites for photocatalytic degradation of dyes under visible light irradiation. On the basis of the experimental data, it proposed a mechanism accounting for the degradation of dye pollutants over GOR-Au under visible light irradiation as schematically illustrated in Fig 5. The dye was firstly excited to dye*, followed by an electron transfer from the dye* to graphene. Then, the electron moved to a gold nanoparticle and was trapped by O_2 to produce various ROSs. The dye+ finally itself degraded and/or was degraded by the ROSs.

The photoactivity of GOR-Au was evaluated using Rhodamine B (RhB) under visible light irradiation, and the results are shown in Fig. 6. It can be seen that RhB was very stable under visible light irradiation without the catalyst or over GOR-Au in the dark. It was slightly degraded in the presence of GOR. However, in the presence of GOR-Au, the RhB degradation was remarkably enhanced; the rate constant was calculated to be about $8.7 * 10^{-3}$ -min^{-1}, much larger than that of P25 ($4.9 * 10^{-3}$ min^{-1}), Au deposited P25 (P25-Au, $5.1 * 10^{-3}$ min^{-1}) and GOR ($5.2 * 10^{-4}$ min^{-1}).

Other non-biodegradable dyes, including methylene blue (MB) and orange II, were also examined using catalyst GOR-Au under visible light irradiation. The rate constants were calculated to be
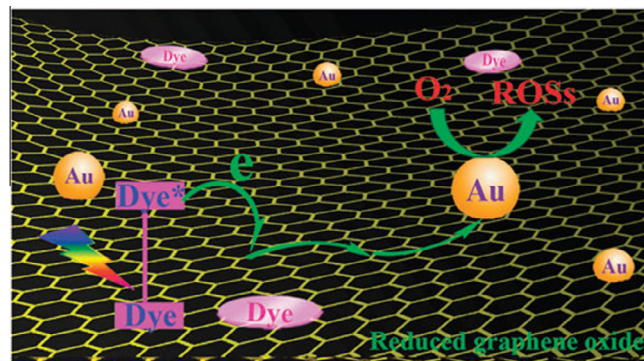

Fig. 5. A proposed mechanism of photosensitized degradation of dyes over GOR-Au under visible light irradiation. (Reproduced with permission from Ref. [254] by The Royal Society of Chemistry.)
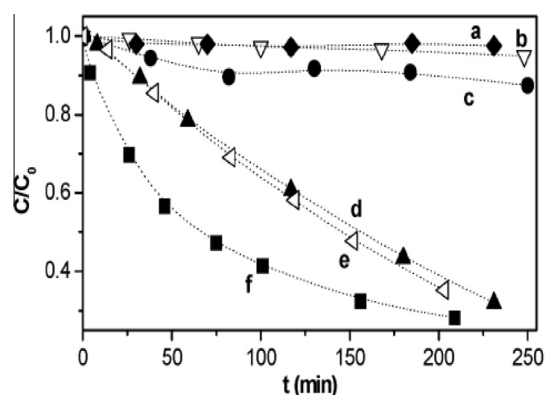

Fig. 6. Degradation of RhB (a) over GOR-Au in the dark, and (b) without catalyst, over (c) GOR, (d) P25, (e) P25-Au and (f) GOR-Au under visible light irradiation. Experimental conditions: 5.3×10^{-3} mM RhB solution and 6.3 mg of photocatalyst material. (Reproduced from Ref. [254] by permission of The Royal Society of Chemistry.)

about $4.1 * 10^{-2}$ min^{-1} and $9.4 * 10^{-4}$ min^{-1} for MB and orange II, respectively. It was noted that the degradation rate for MB was much faster than that for RhB and orange II despite the redox potential of MB* being the highest among the dyes [255]. This was attributed to their different adsorption abilities on GOR-Au,
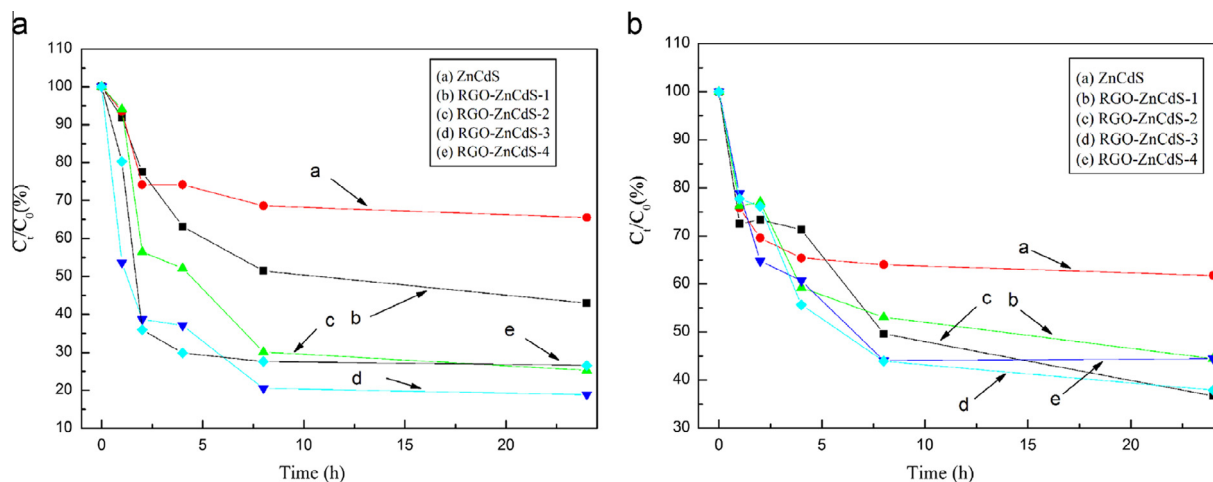

Fig. 4. Degradation curves under visible light irradiation of the samples for methyl orange (A) and RhB (B). Experimental conditions: RGO–ZnCdS nanocomposite (10 mg); methyl orange or RhB solution of (10^{-5} mol/L). (Reproduced from Ref. [251] by permission of Elsevier.) (For interpretation of the references to color in this figure legend, the reader is referred to the web version of this article.)

which were 88.6%, 27.6% and 8.5% for MB, RhB and orange II, respectively. Considering that the electron recombination was greatly depressed on GOR-Au, the high adsorption of MB on the catalyst surface would remarkably enhance the electron transfer efficiency and contact opportunity with surface adsorbed ROSs.

Zhang et al. [256] synthesized the graphene–metal–oxide composites for the degradation of dyes under visible light irradiation. The preparation of metal oxides as SnO₂ and TiO₂ materials onto graphene sheets to prepare the graphene based metal oxide nanocomposites (Fig. 7).

The photocatalytic activity of both samples was evaluated using the degradation of RhB under visible light irradiation. It can be seen from Fig. 8 that RhB was very stable under visible light irradiation without the presence of a photocatalyst. It was slightly degraded in the presence of RGO. However, in the presence of catalysts RGO–SnO₂ and RGO–TiO₂, the degradation was remarkably enhanced with rate constants of about $6.2 * 10^{-3}$ min^{-1} for RGO–SnO₂ and $3.6 * 10^{-3}$ min^{-1} for RGO–TiO₂, significantly higher than that of RGO ($3.9 * 10^{-4}$ min^{-1}). In addition, photocatalyst RGO–SnO₂ performed better than RGO–TiO₂ and commercial product P25.

The presence of reduced graphene sheets greatly enhanced the photocatalytic activity of the metal oxides for the degradation of RhB under visible light irradiation because of the effective charge separation and transfer. The RGO–SnO₂ system exhibited a better photocatalytic activity than P25 and RGO–TiO₂ due to the good electrical conductivity and effective charge separation due to the presence of RGO.

Fan et al. [257] prepared ZnO/reduced graphene oxide hybrids for enhanced photocatalytic degradation of dye wastewater. Xu et al. [258] demonstrated that graphene-hybridized ZnO photocatalysts show enhanced photocatalytic activity for the degradation of organic dye, and the highest photocatalytic activity is about four times as that of pristine ZnO. Kavitha et al. [259] synthesized graphene-ZnO nanoparticle hybrids through the in-situ generation of ZnO nanoparticles onto graphene, and the photocatalytic results showed that over 70% of the methyleneblue (MB) in ethanol was degraded within 3 h under ultraviolet (UV) irradiation.

Fu et al. [260] have investigated the photodegradation of MB using ZnO–graphene nanohybrids, and found that the nanohybrids containing 2.5% graphene exhibit the highest activity, which was
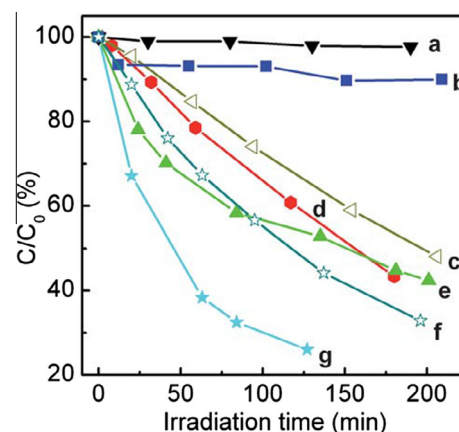

Fig. 8. Degradation of RhB (a) without catalyst, with (b) RGO, (c) RGO–TiO₂, (d) P25, (e) RGO–SnO₂, (f) RGO–TiO₂-400, and (g) RGO– SnO₂-400. Experimental conditions: $5.3 * 10^{-3}$ mM Rhodium B (RhB) solution and 6.3 mg of photocatalyst material. (Reproduced from Ref. [256] by permission of The Royal Society of Chemistry.)

three times as large as that of pure ZnO. The photocatalytic properties of the as-prepared ZnO/rGO hybrids were also investigated through the degradation of MB, methylene orange (MO), and Rhodamine 6 G (Rh6G) under UV irradiations at room temperature [257].

To investigate the photocatalytic properties of the as-prepared ZnO/rGO hybrids, the photodegradation of MB solution (50 mL) was performed using the ZnO/rGO hybrids and pure ZnO synthesized by the same conditions. Results showed that the absorption intensities of the MB solution diminished gradually as the irradiation time increased. Under UV irradiation for 35 min, the absorption peak of MB disappeared completely and the MB solution became colorless, which was much better than previous reports [261,262]. The photocatalytic stability of the as-prepared ZnO/rGO hybrids has also been investigated by four cyclic photo degradations. After four cycles of degradation, the as-prepared ZnO/rGO hybrids did not exhibit any significant loss in photocatalytic activity, indicating good photocatalytic stability during the oxidation of MB molecules. The stable photocatalytic activity may be ascribed to the transfer of the photo-generated electrons from ZnO to rGO. The photodegradation rates of MB solution with pure ZnO and ZnO/rGO hybrids and without catalysts have been analyzed. It was found that the degradation time using the as-prepared ZnO/rGO hybrids was about 1/3 of that of pure ZnO, confirming the enhanced photocatalytic efficiency of ZnO/rGO hybrids. The results show that the as-prepared ZnO/rGO hybrids exhibit higher photocatalytic efficiency than pure ZnO nanostructures, and above 99% dyes in wastewater could be degraded after irradiation for 30 min. This enhanced photocatalytic activity can be attributed to the low recombination probability of photogenerated electron–hole pairs due to efficient charge transfer from ZnO to rGO sheets.

Shanmugam et al. [263] have prepared the graphene-V₂O₅ nanocomposite via hydrothermal method and tested for the degradation of MB dye under direct sunlight. The G-V₂O₅ composite was prepared by solution mixing followed by sonication. Schematic representation of the formation of the G-V₂O₅ nanocomposite is shown in Fig. 9.

The photocatalytic activity of the synthesized G-V₂O₅ nanocomposite was analyzed using MB dye under UV, visible, and direct sunlight irradiations as shown in Fig. 9. The irradiation of UV light for different time intervals and the rate of degradation of MB dye was observed as shown in Fig. 10(a) and Fig. 10(b). The results showed that visible light irradiated MB dye with the G-V₂O₅ nanocomposite solution was degraded quickly within 150 min
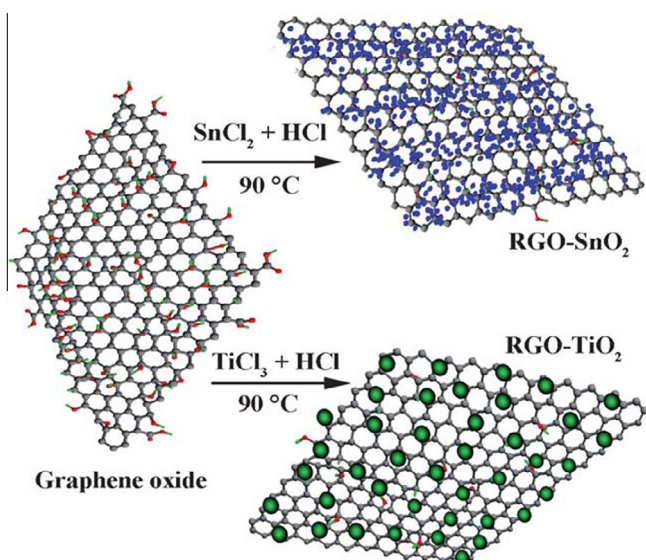

Fig. 7. A scheme showing the preparation of samples RGO–SnO₂ and RGO–TiO₂. (Reproduced from Ref. [256] by permission of The Royal Society of Chemistry.)
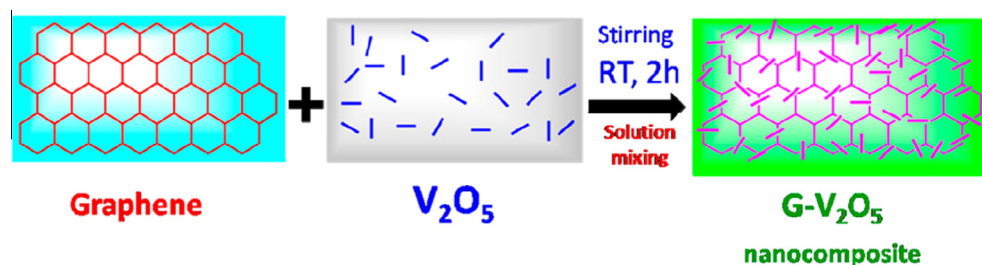
Fig. 9. Schematic representation of the formation of the G-V$_2$O$_5$ nanocomposite. (Reprinted with the permission from Ref. [263] copy right from American Chemical Society).

compared to UV irradiation. Fig. 10(c) showed the absorption spectra of MB dye solution with the G-V$_2$O$_5$ nanocomposite under direct sunlight irradiation for different time intervals. The dye degraded at a faster rate under sunlight (90 min) compared to UV and visible light sources as the sunlight has higher intensity. To demonstrate the influence of graphene on the photodegradation, the degradation of MB with pure V$_2$O$_5$ was studied under visible light. Fig. 10(d) showed the variation of C/C$_0$ with time for V$_2$O$_5$ and the G-V$_2$O$_5$ nanocomposite, where C$_0$ is the initial concentration of the dye solution, and C is the concentration of the dye solution with respect to the degradation time (t). It is obvious from Fig. 10(d) that the rate of degradation was quite faster in the composite compared to pure V$_2$O$_5$ rods, which showed the beneficial impact of graphene on the photocatalytic performance of the composite. The photocatalytic activity of the composite prepared by the present method is higher than the graphene-V$_2$O$_5$ based composite prepared by the hydrothermal method [264].

4. Nanomaterials as antibacterial agents

One of the serious problems world is facing today is infectious diseases and increasing resistance of the microorganisms towards antibiotics [265]. Most of the infection causing bacteria are with strong resistant to at least one of the antibiotics that are generally used to eradicate the infection [266]. For preventing such type of infectious microorganisms, nanoantimicrobials have been proved as effective treatment option [267]. The bacterial growth control
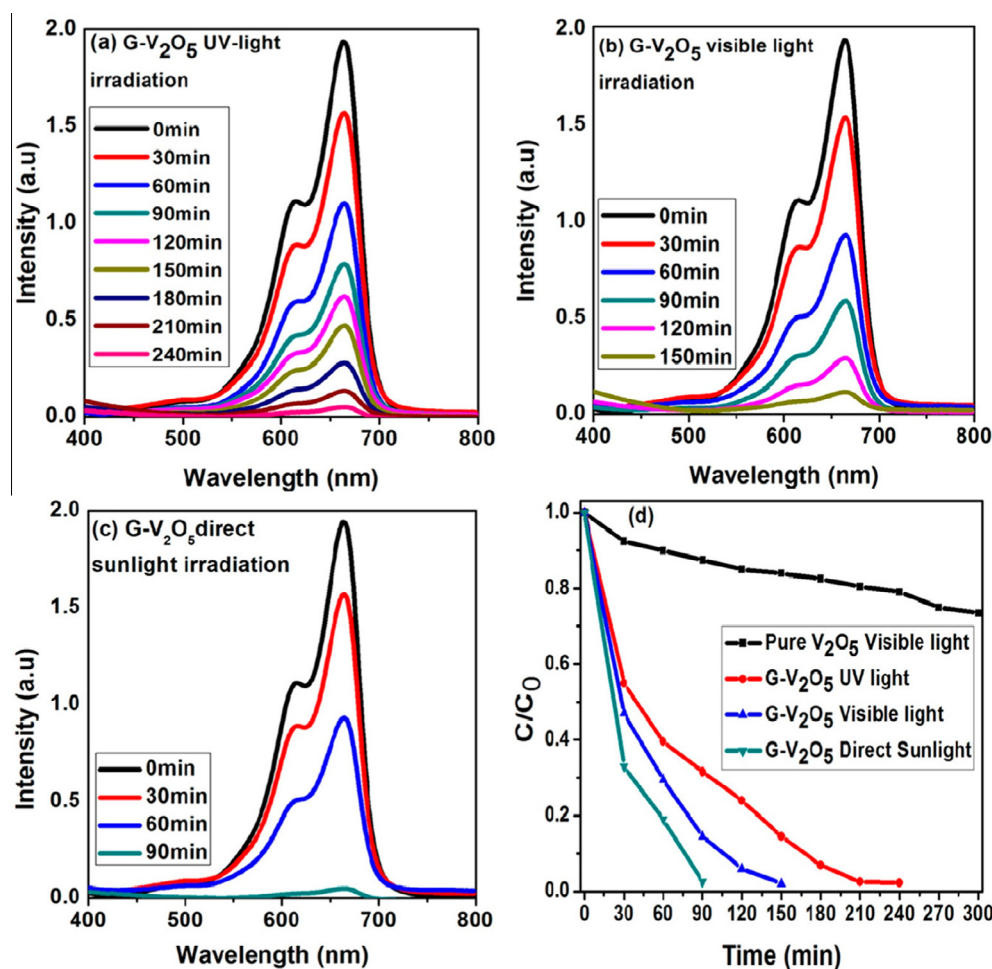

Fig. 10. Photodegradation of MB dye under the irradiation of (a) UV-light, (b) visible light, (c) direct sunlight, and (d) C/C$_0$ vs time (min) for the G-V$_2$O$_5$ nanocomposite. Experimental conditions: 10 mg of photocatalyst material; 50 mL of MB dye solution. (Reprinted with permission from Ref. [263] copy right from American Chemical Society).

is a challenging aspect in every environmental applications, because they are complex media rich in microorganisms and nutrients and their surfaces are exposed for a long period. Liu et al. [268] have discussed about antibacterial activity of graphite (Gt), graphite oxide (GtO), graphene oxide (GO), and reduced graphene oxide (rGO): membrane and oxidative stress. *E. coli* was used as a model bacterium to evaluate antibacterial activities of the four types of graphene-based materials. *E. coli* cells (10^6–10^7 CFU/mL) were incubated with the same concentration (40 μg/mL) of Gt, GtO, GO, and rGO dispersions in isotonic saline solution for 2 h. The death rate of bacterial cells was determined by the colony counting method. The isotonic saline solution without graphene-based materials was used as a control. As shown in Fig. 11(a), Gt dispersion exhibited a moderate cytotoxicity with the cell inactivation percentage at 26.1 ± 4.8%. The GtO dispersion showed a slight weaker antibacterial activity compared with Gt, having the cell inactivation percentage at 15.0 ± 3.7%. GO had a much stronger bacterial activity compared with GtO. The loss of *E. coli* viability increased to 69.3 ± 6.1%, which was more than 4-fold compared with that of GtO. rGO had a lower antibacterial activity compared with GO with a bacterial inactivation percentage of 45.9 ± 4.8%. Significant differences were found in their antibacterial activities among the four materials. In particular, GO and rGO showed much higher bacterial inactivation percentages compared with those of Gt and GtO. Fig. 11(b) indicates the loss of *E. coli* viability steadily increases with extending incubation time. For GO dispersion, the loss of *E. coli* viability increases from 49.1 ± 6.0%, 69.3 ± 6.1%, 81.5 ± 3.9% and 89.7 ± 3.1% after incubation period of 1 h, 2 h, 3 h and 4 h respectively. rGO dispersion displayed a similar trend. The loss of *E. coli* viability was 35.6 ± 2.5%, 47.4 ± 4.6, 67.8 ± 5.6 and 74.9 ± 4.8% after incubation period of 1 h, 2 h, 3 h, and 4 h, respectively. For both materials, a large fraction of cell death occurred in the first hours of incubation. Comparing GO and rGO dispersions, GO dispersions had much higher antibacterial activities than rGO dispersions at all tested incubation intervals. Fig. 11(c), the loss of *E. coli* viability progressively went up with the increases of GO or rGO concentration. The loss of *E. coli* viability jumped from 10.5 ± 6.6% at the GO concentration of 5 μg/mL to 91.6 ± 3.2% at 80 μg/mL. The majority of *E. coli* was killed after incubation with GO at the concentration of 80 μg/mL. In a similar manner, rGO dispersion at the concentration of 5 μg/ mL killed only 8.4 ± 7.3% of *E. coli*, while 80 μg/mL rGO dispersion kills 76.8 ± 3.1% of *E. coli*. Fig. 11(d) shows SEM image of *E. coli* cells which were individually wrapped by thin layers of GO nanosheets.

The correlation among antibacterial activities, GSH oxidation and aggregate size is summarized in Table 8, which can be examined from three aspects.

Firstly, comparing GtO and GO, they have similar capacities in oxidizing GSH (GtO at 21.4 ± 1.1% vs GO at 22.2 ± 0.7%); however, GO dispersion can kill much higher fractions of *E. coli* (69.3 ± 6.6%) than GtO dispersion (15.0 ± 3.7%). GtO and GO contain

Table 8
The correlation among antibacterial activities, oxidative stress and particle size. (Reprinted with permission from Ref. [268] copy right from American Chemical Society).

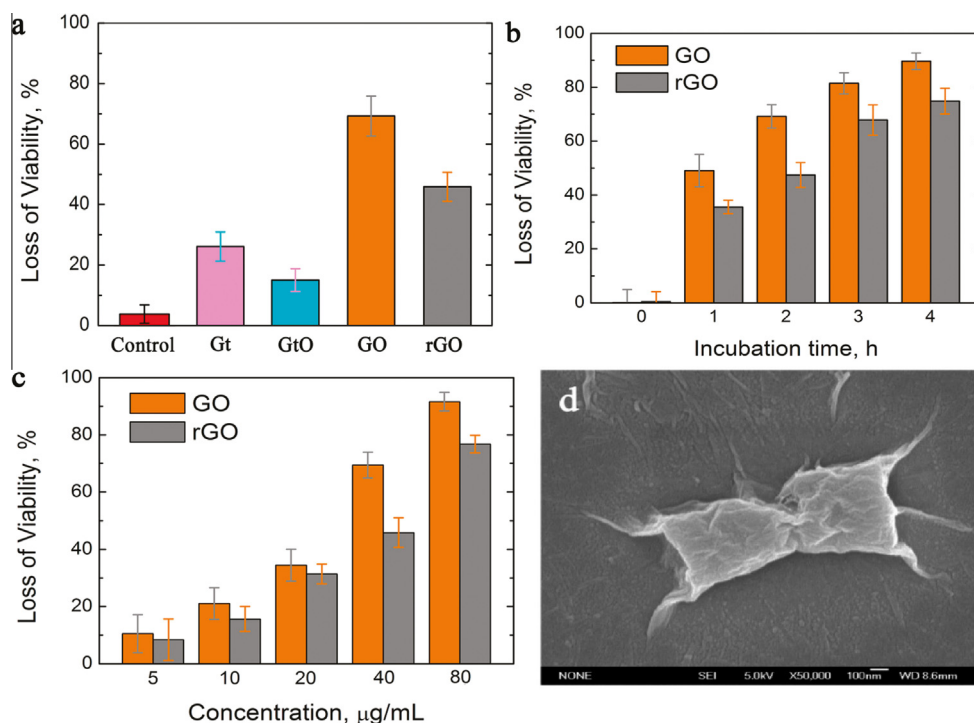| S. No.	Materials	Loss of cells (%)	Loss of GSH (%)	Particle size (μm)
1.	GtO (Graphite Oxide)	15.0 ± 3.7	21.4 ± 1.1	6.28 ± 2.50
2.	Gt (graphite)	26.1 ± 4.8	29.9 ± 0.7	6.87 ± 3.12
3.	rGO (reduced graphene oxide)	45.9 ± 4.8	94.2 ± 1.1	2.75 ± 1.18
4.	GO (graphene oxide)	69.3 ± 6.6	22.2 ± 0.7	0.31 ± 0.20

Fig. 11. (a) Cell viability measurement after incubation with Gt, GtO, GO, and rGO dispersions. A 5 mL portion of graphene-based materials (80 μg/mL) was incubated with *E. coli* (10^6–10^7 colony forming units per milliliter (CFU/mL), 5 mL) for 2 h at 250 rpm shaking speed and 37 °C. Loss of cell viability rates was obtained by colony counting method. Isotonic saline solution without graphene-based materials was used as control. (b) Time-dependent antibacterial activities of GO and rGO; 5 mL of GO or rGO (80 μg/ mL) was incubated with E. coli (10^6–10^7 CFU/mL, 5 mL) for 4 h. The loss of visibility was measured at 0, 1, 2, 3, and 4 h, respectively. (c) Concentration-dependent antibacterial activities of GO and rGO; 5 mL of GO or rGO (at 10, 20, 40, 80, and 160 μg/mL) was incubated with E. coli (10^6–10^7 CFU/mL, 5 mL) for 2 h. (d) E. coli cells after incubation with GO dispersion (40 μg/mL) for 2 h. (Reprinted with permission from Ref. [268] copy right from American Chemical Society).
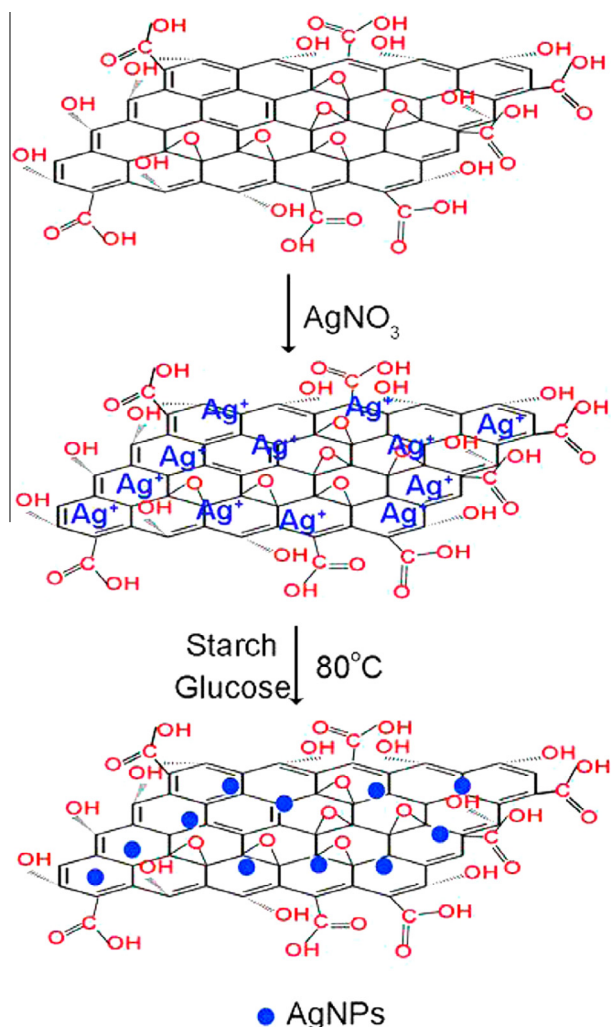
Fig. 12. Schematic of the procedure for preparing GO-Ag nanocomposite. (Reprinted with permission from Ref. [269] copy right from American Chemical Society).

almost the same chemical functional groups. Their difference is that GO is individual nanosheets with average size of $0.31 \pm 0.20 \, \mu m$, while GtO is aggregated stacks of GO nanosheets with average particle size of $6.28 \pm 2.50 \, \mu m$. Their distinct antibacterial activities suggest the aggregation of graphene nanosheets is important in the antibacterial mechanism. Materials having smaller size (e.g., GO), have higher cytotoxicity than those with larger size (e.g., GtO). Second, comparing Gt and GtO, Gt particles ($6.87 \pm 3.12 \, \mu m$) are slightly larger than GtO particles

($6.28 \pm 2.50 \, \mu m$). However, it was found the antibacterial activity of Gt ($26.1 \pm 4.8\%$) is much higher than that of GtO ($15.0 \pm 3.7\%$). This is obviously correlated with their different GSH oxidation capacities. Metallic Gt can oxidize more GSH than insulating GtO, suggesting that the metallicity of graphene materials also played a role in their antibacterial activities. Third, if GO with rGO are compared, although rGO shows much stronger oxidation capacity toward GSH, smaller size GO has much higher antibacterial activity than rGO. Overall, results in Table 8 suggest the antibacterial activities of graphene-based materials are attributed to their dispersibility, size, and oxidization capacity. Their antibacterial mechanism is likely to be the synergy of membrane stress and oxidative stress. The antibacterial activity of Gt, GtO, GO, and rGO aqueous dispersions toward *E. coli* was compared. Colony counting method results show that GO has the highest antibacterial activities, followed by rGO, Gt, and GtO under the same dispersion concentration.

Shao et al. [269] have prepared the silver nanoparticle-decorated graphene oxide nanocomposite using chemical process (Fig. 12).

Two strains including Gram negative *E. coli* ATCC 25922 and Gram-positive *S. aureus* ATCC 6538 were selected for antibacterial tests because they are usually associated with the medical-associated infections [270]. Antibacterial property of GO-Ag nanocomposite was investigated by calculating antibacterial ratios based on the numbers of bacteria colonies incubated with different dosages of GO-Ag nanocomposite at 37 °C after a contact time of 1 h, as shown in Fig. 13(a and b).

It was found that the antibacterial ratio increased with increasing GO-Ag nanocomposite dosages. *anti-E. coli* ratio of 60 μL dosage of GO-Ag nanocomposite reached 98.36%, and the *anti-S. aureus* ratio was 96.18%, respectively. Antibacterial ratios were 100% with more than 60 μL dosage. Therefore, antibacterial behavior of GO-Ag nanocomposite displayed a dose-dependent manner. These results indicate that GO-Ag nanocomposites have excellent antibacterial activities against Gram negative *E. coli* and Gram positive *S. aureus*.

Dinh et al. [271] synthesized the multiwalled carbon nanotubes coated with silver nanoparticles using a modified Tollens process (Fig. 14).

The antibacterial activities of Ag-NPs, MWCNTs, and Ag-MWCNTs nanocomposite were initially assessed with the paper-disc diffusion method, which is widely used for quick antibiotic susceptibility determinations. Fig. 15(a and b) shows the photographs of result of antibacterial test for studied samples using paper-disc diffusion method against Gram-negative *E. coli* and Gram-positive *S. aureus* bacteria. The antibacterial effects of Ag-MWCNTs samples at different silver concentrations were from 10 μg/mL, 20 μg/mL, 30 μg/mL, and 50 μg/mL. The antibacterial ability of pure Ag-NPs sample (30 μg/mL) was also tested for comparison purpose.
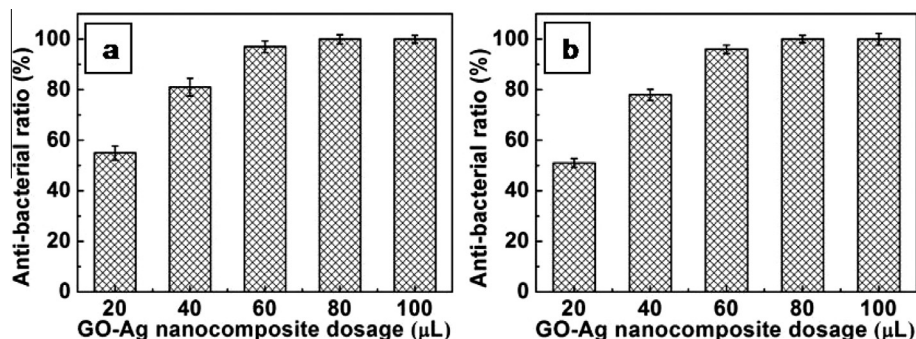

Fig. 13. Antibacterial ratios of *E. coli* and *S. aureus* (a and b). (Reprinted with permission from Ref. [269] copy right from American Chemical Society).
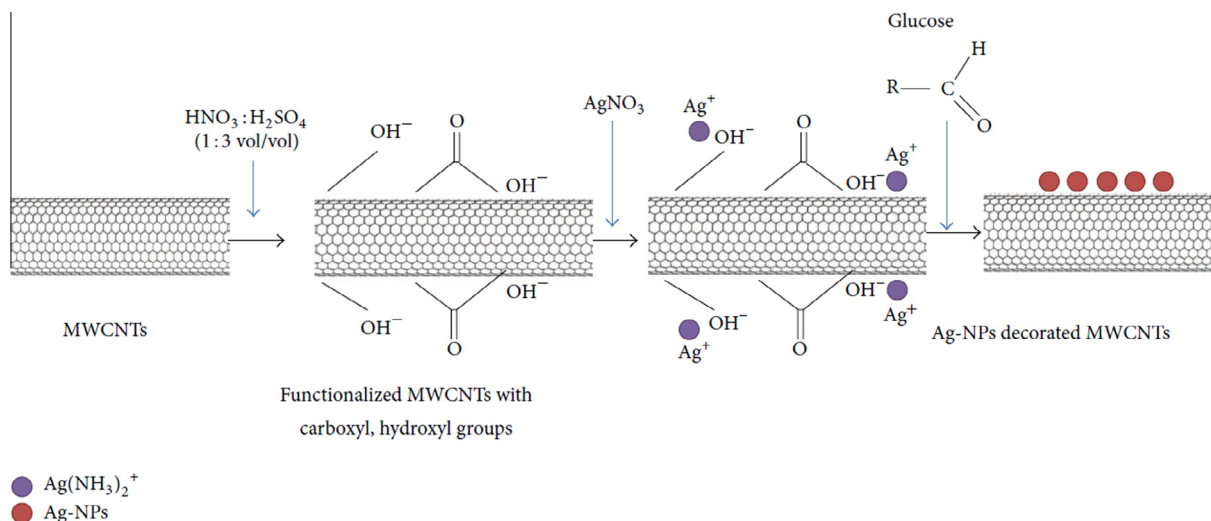
Fig. 14. Two-step protocol for decoration of silver nanoparticles on the multiwalled carbon nanotubes. (Reprinted with permission from Ref. [271] Copyright © 2015).
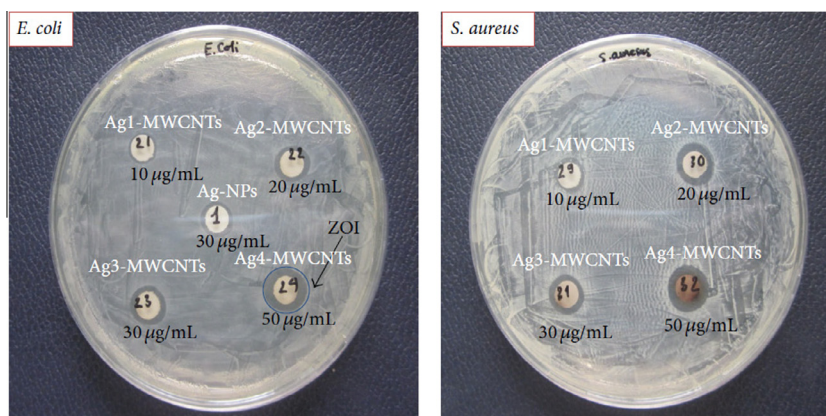

Fig. 15. Antibacterial activity of Ag-MWCNTs samples against *E. coli* and *S. aureus* bacteria. (Reprinted with permission from Ref. [271] Copyright © 2015).

It can be seen that both Ag-NPs and Ag-MWCNTs composite samples were found to exhibit significant inhibitory effect against both *E. coli* and *S. aureus* bacteria. The diameter of zone of inhibition (ZOI) for studied samples was measured. In another study by same researchers, they reported that the Ag-MWCNTs have larger inhibition zone than that of pure Ag-NPs and pristine MWCNTs indicating the higher antibacterial activity of the composite material [272]. This finding suggests that the bacterial growth inhibition of the composite sample might be synergetic effect resulting from both the Ag nanoparticles and MWCNTs. The existence of zone of inhibition suggests that the Ag-MWCNTs could kill the bacteria by direct contact through disruption of bacterial membrane function. It is also emphasized that the antibacterial activity of as-prepared Ag-NPs and Ag- MWCNTs samples was more effective against *E. coli* bacteria than that of *S. aureus* bacteria. This might be from the thinner thickness of the peptidoglycan layer of Gram-negative *E. coli* bacteria as compared to that of the Gram-positive *S. aureus* bacteria.

5. Conclusions and future perspectives

In the present review article, various nanomaterials are reviewed which have been used for water decontamination. The special emphasis in the review has been given on adsorption, pho-

tocatalytic and antimicrobial properties of nanomaterials. As evident from the reviewed literature, a wide range of nanomaterials have been tested for the removal of inorganic and/or organic pollutants. Many nanomaterials eventually present a potent alternative to conventional treatment methods due to increased adsorption and/or photocatalytic activity and substance specificity. However, most applications are not yet ready for the market due to technical challenges (e.g., scale up, system set up), environmental concerns and cost-effectiveness and hence, only a few nanosized commercial products are available in the market. Moreover, there are some other drawbacks associated with nanomaterials use that have to be negotiated. Sometimes, the mass production of nanomaterials, for their practical use, might be a difficult issue. Furthermore, the availability of enormous quantities of nanomaterials at economically viable prices for water treatment purposes can be a serious bottleneck for industrial applications [273]. Another important challenges is to prevent the release of nanomaterials to the environment where they can accumulate for long periods of time. Additionally, it was pointed out by Gehrke and Geiser [274] that no online monitoring systems exist up till now that could provide reliable real-time measurement data on the quality and quantity of nanoparticles present only in trace amounts in water, thus offering a high innovation potential. Nevertheless, nanomaterials could offer great potential in water treatment and environmental

remediation in the coming decades, in particular designing of point-of-use systems, and in the complete degradation of emerging organic contaminants from water and wastewater.

References

[1] A.D.N. Nemerow, Industrial and Hazardous Waste Treatment, Van Nostrand Reinhold, New York, 1991.

[2] H.Y.A.-E.I. Ali, Chiral Pollutants: Distribution, Toxicity and Analysis by Chromatography and Capillary Electrophoresis, John Wiley & Sons, Chichester, UK, 2004.

[3] I.H.R. Helmer, Water Pollution Control – A Guide to the Use of Water Quality Management Principles, E & FN Spon, London, Great Britain, 1997.

[4] T.E.G.J.H. Lehr, J. Pettyjohn DeMarre, Domestic Water Treatment, McGraw-Hill Book Company, New York, 1980.

[5] N.L. Nemerrow, Industrial Water Pollution: Origins, Characteristics, and Treatment, Addison-Wesley Publishing Company, Massachusetts, 1978.

[6] E. Forgacs, T. Cserháti, G. Oros, Removal of synthetic dyes from wastewaters: a review, Environ. Int. 30 (2004) 953–971.

[7] H.S. Rai, M.S. Bhattacharyya, J. Singh, T.K. Bansal, P. Vats, U.C. Banerjee, Removal of dyes from the effluent of textile and dyestuff manufacturing industry: a review of emerging techniques with reference to biological treatment, Crit. Rev. Environ. Sci. Technol. 35 (2005) 219–238.

[8] I. Ali, T.A. Khan, M. Asim, Removal of arsenic from water by electrocoagulation and electrodialysis techniques, Sep. Purif. Rev. 40 (2011) 25–42.

[9] T.A. Saleh, V.K. Gupta, Column with CNT/magnesium oxide composite for lead (II) removal from water, Environ. Sci. Pollut. Res. 19 (2012) 1224–1228.

[10] V.K. Gupta, A. Nayak, Cadmium removal and recovery from aqueous solutions by novel adsorbents prepared from orange peel and Fe_2O_3 nanoparticles, Chem. Eng. J. 180 (2012) 81–90.

[11] T.A. Saleh, V.K. Gupta, Functionalization of tungsten oxide into MWCNT and its application for sunlight-induced degradation of Rhodamine B, J. Colloid Interface Sci. 362 (2011) 337–344.

[12] T.A. Saleh, S. Agarwal, V.K. Gupta, Synthesis of MWCNT/MnO2 and their application for simultaneous oxidation of arsenite and sorption of arsenate, Appl. Catal. B 106 (2011) 46–53.

[13] V.K. Gupta, S. Agarwal, T.A. Saleh, Synthesis and characterization of alumina-coated carbon nanotubes and their application for lead removal, J. Hazard. Mater. 185 (2011) 17–23.

[14] I.S.M.C. Sanady, Health damage due to pollution in Hungary, in: Proceedings of the Rome Symposium, International Association of Hydrological Sciences, Wallingford, Oxfordshire, UK, 1995.

[15] J. Matschullat, Arsenic in the geosphere — a review, Sci. Total Environ. 249 (2000) 297–312.

[16] V.K. Gupta, A. Imran, Water treatment: low-cost alternatives to carbon adsorbents, in: Encyclopedia of Surface and Colloid Science, third ed., Taylor & Francis, 2015, pp. 7618–7652.

[17] C.K.J.I. Ali, Wastewater treatment and recycling technologies, in: Water Encyclopedia: Domestic, Municipal, and Industrial Water Supply and Waste Disposal, John Wiley & Sons, New York, 2005.

[18] A. Bhatnagar, M. Sillanpää, Utilization of agro-industrial and municipal waste materials as potential adsorbents for water treatment – a review, Chem. Eng. J. 157 (2010) 277–296.

[19] R.K. Gautam, M.C. Chattopadhyaya, Nanomaterials for Wastewater Remediation, 1st Edi., Butterworth-Heinemann, 2016.

[20] V.K.K. Upadhyayula, S. Deng, M.C. Mitchell, G.B. Smith, Application of carbon nanotube technology for removal of contaminants in drinking water: a review, Sci. Total Environ. 408 (2009) 1–13.

[21] P. Xu, G.M. Zeng, D.L. Huang, C.L. Feng, S. Hu, M.H. Zhao, C. Lai, Z. Wei, C. Huang, G.X. Xie, Z.F. Liu, Use of iron oxide nanomaterials in wastewater treatment: a review, Sci. Total Environ. 424 (2012) 1–10.

[22] D. Pathania, P. Singh, Nanosized Metal Oxide-Based Adsorbents for Heavy Metal Removal: A Review, Advanced Materials for Agriculture, Food, and Environmental Safety, John Wiley & Sons Inc., 2014, pp. 243–263.

[23] A.W. Carpenter, C.-F. de Lannoy, M.R. Wiesner, Cellulose nanomaterials in water treatment technologies, Environ. Sci. Technol. 49 (2015) 5277–5287.

[24] N.M. Mubarak, J.N. Sahu, E.C. Abdullah, N.S. Jayakumar, Removal of heavy metals from wastewater using carbon nanotubes, Sep. Purif. Rev. 43 (2014) 311–338.

[25] S. Wang, H. Sun, H.M. Ang, M.O. Tadé, Adsorptive remediation of environmental pollutants using novel graphene-based nanomaterials, Chem. Eng. J. 226 (2013) 336–347.

[26] M. Stefaniuk, P. Oleszczuk, Y.S. Ok, Review on nano zerovalent iron (nZVI): from synthesis to environmental applications, Chem. Eng. J. 287 (2016) 618–632.

[27] Y. Sharma, V. Srivastava, V. Singh, S. Kaul, C. Weng, Nano-adsorbents for the removal of metallic pollutants from water and wastewater, Environ. Technol. 30 (2009) 583–609.

[28] K.B. Tan, M. Vakili, B.A. Horri, P.E. Poh, A.Z. Abdullah, B. Salamatinia, Adsorption of dyes by nanomaterials: recent developments and adsorption mechanisms, Sep. Purif. Technol. 150 (2015) 229–242.

[29] A. Cincinelli, T. Martellini, E. Coppini, D. Fibbi, A. Katsoyiannis, Nanotechnologies for removal of pharmaceuticals and personal care products from water and wastewater. A review, J. Nanosci. Nanotechnol. 15 (2015) 3333–3347.

[30] S. Pacheco, M. Medina, F. Valencia, J. Tapia, Removal of inorganic mercury from polluted water using structured nanoparticles, J. Environ. Eng. 132 (2006) 342–349.

[31] K. Yang, B. Xing, Desorption of polycyclic aromatic hydrocarbons from carbon nanomaterials in water, Environ. Pollut. 145 (2007) 529–537.

[32] K. Hristovski, A. Baumgardner, P. Westerhoff, Selecting metal oxide nanomaterials for arsenic removal in fixed bed columns: from nanopowders to aggregated nanoparticle media, J. Hazard. Mater. 147 (2007) 265–274.

[33] A. Khaleel, P.N. Kapoor, K.J. Klabunde, Nanocrystalline metal oxides as new adsorbents for air purification, Nanostruct. Mater. 11 (1999) 459–468.

[34] L. Li, M. Fan, R. Brown, J. Van Leeuwen, J. Wang, W. Wang, Y. Song, P. Zhang, Synthesis, properties, and environmental applications of nanoscale iron-based materials: a review, Crit. Rev. Environ. Sci. Technol. 36 (2006) 405–431.

[35] X.-Q. Li, D.W. Elliott, W.-X. Zhang, Zero-valent iron nanoparticles for abatement of environmental pollutants: materials and engineering aspects, Crit. Rev. Solid State Mater. Sci. 31 (2006) 111–122.

[36] W.-X. Zhang, Nanoscale iron particles for environmental remediation: an overview, J. Nanopart. Res. 5 (2003) 323–332.

[37] P.G. Tratnyek, R.L. Johnson, Nanotechnologies for environmental cleanup, Nano Today 1 (2006) 44–48.

[38] A.-F. Ngomsik, A. Bee, M. Draye, G. Cote, V. Cabuil, Magnetic nano- and microparticles for metal removal and environmental applications: a review, C.R. Chim. 8 (2005) 963–970.

[39] A. Vaseashta, M. Vaclavikova, S. Vaseashta, G. Gallios, P. Roy, O. Pummakarnchana, Nanostructures in environmental pollution detection, monitoring, and remediation, Sci. Technol. Adv. Mater. 8 (2007) 47–59.

[40] A. Jusoh, L. Su Shiung, N.A. Ali, M.J.M.M. Noor, EuroMed 2006A simulation study of the removal efficiency of granular activated carbon on cadmium and lead, Desalination 206 (2007) 9–16.

[41] S. Wang, Y. Peng, Natural zeolites as effective adsorbents in water and wastewater treatment, Chem. Eng. J. 156 (2010) 11–24.

[42] W.S. Wan Ngah, L.C. Teong, M.A.K.M. Hanafiah, Adsorption of dyes and heavy metal ions by chitosan composites: a review, Carbohydr. Polym. 83 (2011) 1446–1456.

[43] S. Sen Gupta, K.G. Bhattacharyya, Adsorption of heavy metals on kaolinite and montmorillonite: a review, Phys. Chem. Chem. Phys. 14 (2012) 6698–6723.

[44] A.A. Adeyemo, I.O. Adeoye, O.S. Bello, Metal organic frameworks as adsorbents for dye adsorption: overview, prospects and future challenges, Toxicol. Environ. Chem. 94 (2012) 1846–1863.

[45] Y. Kim, J. Yi, Advances in environmental technologies via the application of mesoporous materials, J. Ind. Eng. Chem. 10 (2004) 41–51.

[46] X. Ren, C. Chen, M. Nagatsu, X. Wang, Carbon nanotubes as adsorbents in environmental pollution management: a review, Chem. Eng. J. 170 (2011) 395–410.

[47] G.P. Rao, C. Lu, F. Su, Sorption of divalent metal ions from aqueous solution by carbon nanotubes: a review, Sep. Purif. Technol. 58 (2007) 224–231.

[48] M.B. Seymour, C. Su, Y. Gao, Y. Lu, Y. Li, Characterization of carbon nano-onions for heavy metal ion remediation, J. Nanopart. Res. 14 (2012) 1–13.

[49] S. Wang, C.W. Ng, W. Wang, Q. Li, L. Li, A Comparative study on the adsorption of acid and reactive dyes on multiwall carbon nanotubes in single and binary dye systems, J. Chem. Eng. Data 57 (2012) 1563–1569.

[50] K. Yang, L. Zhu, B. Xing, Adsorption of polycyclic aromatic hydrocarbons by carbon nanomaterials, Environ. Sci. Technol. 40 (2006) 1855–1861.

[51] X. Wang, J. Lu, B. Xing, Sorption of organic contaminants by carbon nanotubes: influence of adsorbed organic matter, Environ. Sci. Technol. 42 (2008) 3207–3212.

[52] A. Stafiej, K. Pyrzynska, Solid phase extraction of metal ions using carbon nanotubes, Microchem. J. 89 (2008) 29–33.

[53] Y.-H. Li, S. Wang, J. Wei, X. Zhang, C. Xu, Z. Luan, D. Wu, B. Wei, Lead adsorption on carbon nanotubes, Chem. Phys. Lett. 357 (2002) 263–266.

[54] C. Lu, C. Liu, Removal of nickel(II) from aqueous solution by carbon nanotubes, J. Chem. Technol. Biotechnol. 81 (2006) 1932–1940.

[55] Y.-H. Li, J. Ding, Z. Luan, Z. Di, Y. Zhu, C. Xu, D. Wu, B. Wei, Competitive adsorption of Pb^{2+}, Cu^{2+} and Cd^{2+} ions from aqueous solutions by multiwalled carbon nanotubes, Carbon 41 (2003) 2787–2792.

[56] K. Anitha, S. Namsani, J.K. Singh, Removal of heavy metal ions using a functionalized single-walled carbon nanotube: a molecular dynamics study, J. Phys. Chem. A 119 (2015) 8349–8358.

[57] C. Lu, H. Chiu, Adsorption of zinc(II) from water with purified carbon nanotubes, Chem. Eng. Sci. 61 (2006) 1138–1145.

[58] C. Lu, Y.-L. Chung, K.-F. Chang, Adsorption of trihalomethanes from water with carbon nanotubes, Water Res. 39 (2005) 1183–1189.

[59] V.K. Gupta, S. Agarwal, T.A. Saleh, Chromium removal by combining the magnetic properties of iron oxide with adsorption properties of carbon nanotubes, Water Res. 45 (2011) 2207–2212.

[60] C.-H. Wu, Adsorption of reactive dye onto carbon nanotubes: equilibrium, kinetics and thermodynamics, J. Hazard. Mater. 144 (2007) 93–100.

[61] S. Chatterjee, M.W. Lee, S.H. Woo, Adsorption of congo red by chitosan hydrogel beads impregnated with carbon nanotubes, Bioresour. Technol. 101 (2010) 1800–1806.

[62] E. Bazrafshan, F.K. Mostafapour, A.R. Hosseini, A. Raksh Khorshid, A.H. Mahvi, Decolorisation of reactive red 120 dye by using single-walled carbon nanotubes in aqueous solutions, J. Chem. 2013 (2013) 8.

[63] Q. Liao, J. Sun, L. Gao, The adsorption of resorcinol from water using multi-walled carbon nanotubes, Colloids Surf. A 312 (2008) 160–165.

[64] G.-C. Chen, X.-Q. Shan, Z.-G. Pei, H. Wang, L.-R. Zheng, J. Zhang, Y.-N. Xie, Adsorption of diuron and dichlobenil on multiwalled carbon nanotubes as affected by lead, J. Hazard. Mater. 188 (2011) 156–163.

[65] H. Hyung, J.-H. Kim, Natural organic matter (nom) adsorption to multi-walled carbon nanotubes: effect of nom characteristics and water quality parameters, Environ. Sci. Technol. 42 (2008) 4416–4421.

[66] L. Joseph, J.R.V. Flora, Y.-G. Park, M. Badawy, H. Saleh, Y. Yoon, Removal of natural organic matter from potential drinking water sources by combined coagulation and adsorption using carbon nanomaterials, Sep. Purif. Technol. 95 (2012) 64–72.

[67] C. Lu, Y.-L. Chung, K.-F. Chang, Adsorption thermodynamic and kinetic studies of trihalomethanes on multiwalled carbon nanotubes, J. Hazard. Mater. 138 (2006) 304–310.

[68] A.W. Morawski, R. Kalenczuk, M. Inagaki, Adsorption of trihalomethanes (THMs) onto carbon spheres, Desalination 130 (2000) 107–112.

[69] W. Chen, L. Duan, D. Zhu, Adsorption of polar and nonpolar organic chemicals to carbon nanotubes, Environ. Sci. Technol. 41 (2007) 8295–8300.

[70] C. Lu, F. Su, S. Hu, Surface modification of carbon nanotubes for enhancing BTEX adsorption from aqueous solutions, Appl. Surf. Sci. 254 (2008) 7035–7041.

[71] B. Pan, B. Xing, Adsorption mechanisms of organic chemicals on carbon nanotubes, Environ. Sci. Technol. 42 (2008) 9005–9013.

[72] C. Chen, X. Wang, Adsorption of Ni(II) from aqueous solution using oxidized multiwall carbon nanotubes, Ind. Eng. Chem. Res. 45 (2006) 9144–9149.

[73] K. Yang, W. Wu, Q. Jing, L. Zhu, Aqueous adsorption of aniline, phenol, and their substitutes by multi-walled carbon nanotubes, Environ. Sci. Technol. 42 (2008) 7931–7936.

[74] Y. Yao, H. Bing, X. Feifei, C. Xiaofeng, Equilibrium and kinetic studies of methyl orange adsorption on multiwalled carbon nanotubes, Chem. Eng. J. 170 (2011) 82–89.

[75] J. Ma, F. Yu, L. Zhou, L. Jin, M. Yang, J. Luan, Y. Tang, H. Fan, Z. Yuan, J. Chen, Enhanced adsorptive removal of methyl orange and methylene blue from aqueous solution by alkali-activated multiwalled carbon nanotubes, ACS Appl. Mater. Interfaces 4 (2012) 5749–5760.

[76] S. Wang, C.W. Ng, W. Wang, Q. Li, Z. Hao, Synergistic and competitive adsorption of organic dyes on multiwalled carbon nanotubes, Chem. Eng. J. 197 (2012) 34–40.

[77] O. Moradi, Adsorption behavior of basic red 46 by single-walled carbon nanotubes surfaces, Fullerenes Nanotubes Carbon Nanostruct. 21 (2013) 286–301.

[78] L. Zhang, X. Song, X. Liu, L. Yang, F. Pan, J. Lv, Studies on the removal of tetracycline by multi-walled carbon nanotubes, Chem. Eng. J. 178 (2011) 26–33.

[79] L. Zhang, T. Xu, X. Liu, Y. Zhang, H. Jin, Adsorption behavior of multi-walled carbon nanotubes for the removal of olaquindox from aqueous solutions, J. Hazard. Mater. 197 (2011) 389–396.

[80] A. Mehrizad, M. Aghaie, P. Gharbani, S. Dastmalchi, M. Monajjemi, K. Zare, Comparison of 4-chloro-2-nitrophenol adsorption on single-walled and multi-walled carbon nanotubes, Iran. J. Environ. Health Sci. Eng. 9 (2012) 1.

[81] J.C. Lou, M.J. Jung, H.W. Yang, J.Y. Han, W.H. Huang, Removal of dissolved organic matter (DOM) from raw water by single-walled carbon nanotubes (SWCNTs), J. Environ. Sci. Health Part A 46 (2011) 1357–1365.

[82] F. Yu, Y. Wu, X. Li, J. Ma, Kinetic and thermodynamic studies of toluene, ethylbenzene, and m-xylene adsorption from aqueous solutions onto KOH-activated multiwalled carbon nanotubes, J. Agric. Food Chem. 60 (2012) 12245–12253.

[83] D. Zhao, W. Zhang, C. Chen, X. Wang, Adsorption of methyl orange dye onto multiwalled carbon nanotubes, Procedia Environ. Sci. 18 (2013) 890–895.

[84] H. Zhu, R. Jiang, L. Xiao, G. Zeng, Preparation, characterization, adsorption kinetics and thermodynamics of novel magnetic chitosan enwrapping nanosized γ-Fe_2O_3 and multi-walled carbon nanotubes with enhanced adsorption properties for methyl orange, Bioresour. Technol. 101 (2010) 5063–5069.

[85] S. Álvarez-Torrellas, A. Rodríguez, G. Ovejero, J. García, Comparative adsorption performance of ibuprofen and tetracycline from aqueous solution by carbonaceous materials, Chem. Eng. J. 283 (2016) 936–947.

[86] J. Ma, Y. Zhuang, F. Yu, Facile method for the synthesis of a magnetic CNTs–C@Fe–chitosan composite and its application in tetracycline removal from aqueous solutions, Phys. Chem. Chem. Phys. 17 (2015) 15936–15944.

[87] M.C. Ncibi, M. Sillanpää, Optimized removal of antibiotic drugs from aqueous solutions using single, double and multi-walled carbon nanotubes, J. Hazard. Mater. 298 (2015) 102–110.

[88] F. Wang, W. Sun, W. Pan, N. Xu, Adsorption of sulfamethoxazole and 17β-estradiol by carbon nanotubes/$CoFe_2O_4$ composites, Chem. Eng. J. 274 (2015) 17–29.

[89] Q. Yang, G. Chen, J. Zhang, H. Li, Adsorption of sulfamethazine by multi-walled carbon nanotubes: effects of aqueous solution chemistry, RSC Adv. 5 (2015) 25541–25549.

[90] W. Yang, Y. Lu, F. Zheng, X. Xue, N. Li, D. Liu, Adsorption behavior and mechanisms of norfloxacin onto porous resins and carbon nanotube, Chem. Eng. J. 179 (2012) 112–118.

[91] M.F.L. De Volder, S.H. Tawfick, R.H. Baughman, A.J. Hart, Carbon nanotubes: present and future commercial applications, Science 339 (2013) 535–539.

[92] L. Ji, W. Chen, L. Duan, D. Zhu, Mechanisms for strong adsorption of tetracycline to carbon nanotubes: a comparative study using activated carbon and graphite as adsorbents, Environ. Sci. Technol. 43 (2009) 2322–2327.

[93] Q. Cong, X. Yuan, J. Qu, A review on the removal of antibiotics by carbon nanotubes, Water Sci. Technol. 68 (2013) 1679–1687.

[94] X. Qu, P.J. Alvarez, Q. Li, Applications of nanotechnology in water and wastewater treatment, Water Res. 47 (2013) 3931–3946.

[95] R. Sitko, B. Zawisza, E. Malicka, Graphene as a new sorbent in analytical chemistry, TrAC, Trends Anal. Chem. 51 (2013) 33–43.

[96] A. Stafiej, K. Pyrzynska, Adsorption of heavy metal ions with carbon nanotubes, Sep. Purif. Technol. 58 (2007) 49–52.

[97] J. Zhao, Z. Wang, J.C. White, B. Xing, Graphene in the aquatic environment: adsorption, dispersion, toxicity and transformation, Environ. Sci. Technol. 48 (2014) 9995–10009.

[98] G. Zhao, J. Li, X. Ren, C. Chen, X. Wang, Few-layered graphene oxide nanosheets as superior sorbents for heavy metal ion pollution management, Environ. Sci. Technol. 45 (2011) 10454–10462.

[99] W. Wu, Y. Yang, H. Zhou, T. Ye, Z. Huang, R. Liu, Y. Kuang, Highly efficient removal of Cu(II) from aqueous solution by using graphene oxide, Water Air Soil Pollut. 224 (2012) 1–8.

[100] R. Sitko, E. Turek, B. Zawisza, E. Malicka, E. Talik, J. Heimann, A. Gagor, B. Feist, R. Wrzalik, Adsorption of divalent metal ions from aqueous solutions using graphene oxide, Dalton Trans. 42 (2013) 5682–5689.

[101] G. Zhao, X. Ren, X. Gao, X. Tan, J. Li, C. Chen, Y. Huang, X. Wang, Removal of Pb (ii) ions from aqueous solutions on few-layered graphene oxide nanosheets, Dalton Trans. 40 (2011) 10945–10952.

[102] Z.-H. Huang, X. Zheng, W. Lv, M. Wang, Q.-H. Yang, F. Kang, Adsorption of lead (II) ions from aqueous solution on low-temperature exfoliated graphene nanosheets, Langmuir 27 (2011) 7558–7562.

[103] Y.-C. Lee, J.-W. Yang, Self-assembled flower-like TiO_2 on exfoliated graphite oxide for heavy metal removal, J. Ind. Eng. Chem. 18 (2012) 1178–1185.

[104] J. Li, S. Zhang, C. Chen, G. Zhao, X. Yang, J. Li, X. Wang, Removal of Cu(II) and fulvic acid by graphene oxide nanosheets decorated with Fe_3O_4 nanoparticles, ACS Appl. Mater. Interfaces 4 (2012) 4991–5000.

[105] Y. Wang, S. Liang, B. Chen, F. Guo, S. Yu, Y. Tang, Synergistic removal of Pb(II), Cd(II) and humic acid by Fe_3O_4@mesoporous silica-graphene oxide composites, PLoS One 8 (2013) e65634.

[106] X.-J. Hu, Y.-G. Liu, G.-M. Zeng, S.-H. You, H. Wang, X. Hu, Y.-M. Guo, X.-F. Tan, F.-Y. Guo, Effects of background electrolytes and ionic strength on enrichment of Cd(II) ions with magnetic graphene oxide–supported sulfanilic acid, J. Colloid Interface Sci. 435 (2014) 138–144.

[107] S. Kumar, R.R. Nair, P.B. Pillai, S.N. Gupta, M.A.R. Iyengar, A.K. Sood, Graphene oxide–MnFe2O4 magnetic nanohybrids for efficient removal of lead and arsenic from water, ACS Appl. Mater. Interfaces 6 (2014) 17426–17436.

[108] Y. Zhang, L. Yan, W. Xu, X. Guo, L. Cui, L. Gao, Q. Wei, B. Du, Adsorption of Pb (II) and Hg(II) from aqueous solution using magnetic $CoFe_2O_4$-reduced graphene oxide, J. Mol. Liq. 191 (2014) 177–182.

[109] D. Nandi, T. Basu, S. Debnath, A.K. Ghosh, A. De, U.C. Ghosh, Mechanistic insight for the sorption of Cd(II) and Cu(II) from aqueous solution on magnetic Mn-doped Fe(III) oxide nanoparticle implanted graphene, J. Chem. Eng. Data 58 (2013) 2809–2818.

[110] X.-J. Hu, Y.-G. Liu, H. Wang, A.-W. Chen, G.-M. Zeng, S.-M. Liu, Y.-M. Guo, X. Hu, T.-T. Li, Y.-Q. Wang, L. Zhou, S.-H. Liu, Removal of Cu(II) ions from aqueous solution using sulfonated magnetic graphene oxide composite, Sep. Purif. Technol. 108 (2013) 189–195.

[111] J. Hur, J. Shin, J. Yoo, Y.-S. Seo, Competitive adsorption of metals onto magnetic graphene oxide: comparison with other carbonaceous adsorbents, Sci. World J. 2015 (2015) 11.

[112] C.J. Madadrang, H.Y. Kim, G. Gao, N. Wang, J. Zhu, H. Feng, M. Gorring, M.L. Kasner, S. Hou, Adsorption behavior of EDTA-graphene oxide for Pb (II) removal, ACS Appl. Mater. Interfaces 4 (2012) 1186–1193.

[113] L. Hao, H. Song, L. Zhang, X. Wan, Y. Tang, Y. Lv, SiO2/graphene composite for highly selective adsorption of Pb(II) ion, J. Colloid Interface Sci. 369 (2012) 381–387.

[114] T.S. Sreeprasad, S.M. Maliyekkal, K.P. Lisha, T. Pradeep, Reduced graphene oxide–metal/metal oxide composites: facile synthesis and application in water purification, J. Hazard. Mater. 186 (2011) 921–931.

[115] X. Zhang, C. Cheng, J. Zhao, L. Ma, S. Sun, C. Zhao, Polyethersulfone enwrapped graphene oxide porous particles for water treatment, Chem. Eng. J. 215 (2013) 72–81.

[116] G. Xie, P. Xi, H. Liu, F. Chen, L. Huang, Y. Shi, F. Hou, Z. Zeng, C. Shao, J. Wang, A facile chemical method to produce superparamagnetic graphene oxide–Fe_3O_4 hybrid composite and its application in the removal of dyes from aqueous solution, J. Mater. Chem. 22 (2012) 1033–1039.

[117] S. Bai, X. Shen, X. Zhong, Y. Liu, G. Zhu, X. Xu, K. Chen, One-pot solvothermal preparation of magnetic reduced graphene oxide-ferrite hybrids for organic dye removal, Carbon 50 (2012) 2337–2346.

[118] F. Liu, S. Chung, G. Oh, T.S. Seo, Three-dimensional graphene oxide nanostructure for fast and efficient water-soluble dye removal, ACS Appl. Mater. Interfaces 4 (2012) 922–927.

[119] Y. Liu, Y. Hu, M. Zhou, H. Qian, X. Hu, Microwave-assisted non-aqueous route to deposit well-dispersed ZnO nanocrystals on reduced graphene oxide sheets with improved photoactivity for the decolorization of dyes under visible light, Appl. Catal. B 125 (2012) 425–431.

1135

[120] H. Fan, X. Zhao, J. Yang, X. Shan, L. Yang, Y. Zhang, X. Li, M. Gao, ZnO–graphene composite for photocatalytic degradation of methylene blue dye, Catal. Commun. 29 (2012) 29–34.
[121] H.R. Pant, C.H. Park, P. Pokharel, L.D. Tijing, C.S. Kim, ZnO micro-flowers assembled on reduced graphene sheets with high photocatalytic activity for removal of pollutants, Powder Technol. 235 (2013) 853–858.
[122] X. Wang, H. Tian, Y. Yang, H. Wang, S. Wang, W. Zheng, Y. Liu, Reduced graphene oxide/CdS for efficiently photocatalystic degradation of methylene blue, J. Alloy. Compd. 524 (2012) 5–12.
[123] L.M. Pastrana-Martínez, S. Morales-Torres, V. Likodimos, J.L. Figueiredo, J.L. Faria, P. Falaras, A.M. Silva, Advanced nanostructured photocatalysts based on reduced graphene oxide–TiO₂ composites for degradation of diphenhydramine pharmaceutical and methyl orange dye, Appl. Catal. B 123 (2012) 241–256.
[124] Y. Yao, S. Miao, S. Liu, L.P. Ma, H. Sun, S. Wang, Synthesis, characterization, and adsorption properties of magnetic Fe₃O₄@ graphene nanocomposite, Chem. Eng. J. 184 (2012) 326–332.
[125] P. Bradder, S.K. Ling, S. Wang, S. Liu, Dye adsorption on layered graphite oxide, J. Chem. Eng. Data 56 (2010) 138–141.
[126] T. Liu, Y. Li, Q. Du, J. Sun, Y. Jiao, G. Yang, Z. Wang, Y. Xia, W. Zhang, K. Wang, Adsorption of methylene blue from aqueous solution by graphene, Colloids Surf. B 90 (2012) 197–203.
[127] Y. Gao, Y. Li, L. Zhang, H. Huang, J. Hu, S.M. Shah, X. Su, Adsorption and removal of tetracycline antibiotics from aqueous solution by graphene oxide, J. Colloid Interface Sci. 368 (2012) 540–546.
[128] Y. Lin, S. Xu, J. Li, Fast and highly efficient tetracyclines removal from environmental waters by graphene oxide functionalized magnetic particles, Chem. Eng. J. 225 (2013) 679–685.
[129] L. Zhao, F. Xue, B. Yu, J. Xie, X. Zhang, R. Wu, R. Wang, Z. Hu, S.-T. Yang, J. Luo, TiO₂–graphene sponge for the removal of tetracycline, J. Nanopart. Res. 17 (2015) 1–9.
[130] E.E. Ghadim, F. Manouchehri, G. Soleimani, H. Hosseini, S. Kimiagar, S. Nafisi, Adsorption properties of tetracycline onto graphene oxide: equilibrium, kinetic and thermodynamic studies, PLoS One 8 (2013) e79254.
[131] H. Chen, B. Gao, H. Li, Removal of sulfamethoxazole and ciprofloxacin from aqueous solutions by graphene oxide, J. Hazard. Mater. 282 (2015) 201–207.
[132] F. Yu, J. Ma, D. Bi, Enhanced adsorptive removal of selected pharmaceutical antibiotics from aqueous solution by activated graphene, Environ. Sci. Pollut. Res. 22 (2015) 4715–4724.
[133] J. Ma, M. Yang, F. Yu, J. Zheng, Water-enhanced removal of ciprofloxacin from water by porous graphene hydrogel, Sci. Rep. 5 (2015).
[134] X. Hu, Q. Zhou, Health and ecosystem risks of graphene, Chem. Rev. 113 (2013) 3815–3835.
[135] C. Bussy, H. Ali-Boucetta, K. Kostarelos, Safety considerations for graphene: lessons learnt from carbon nanotubes, Acc. Chem. Res. 46 (2012) 692–701.
[136] A. Bianco, Graphene: safe or toxic? The two faces of the medal, Angew. Chem. Int. Ed. 52 (2013) 4986–4997.
[137] J.E. Van Benschoten, B.E. Reed, M.R. Matsumoto, P.J. McGarvey, Metal removal by soil washing for an iron oxide coated sandy soil, Water Environ. Res. 66 (1994) 168–174.
[138] J.A. Coston, C.C. Fuller, J.A. Davis, Pb²⁺ and Zn²⁺ adsorption by a natural aluminum- and iron-bearing surface coating on an aquifer sand, Geochim. Cosmochim. Acta 59 (1995) 3535–3547.
[139] A. Agrawal, K.K. Sahu, Kinetic and isotherm studies of cadmium adsorption on manganese nodule residue, J. Hazard. Mater. 137 (2006) 915–924.
[140] A. Henglein, Small-particle research: physicochemical properties of extremely small colloidal metal and semiconductor particles, Chem. Rev. 89 (1989) 1861–1873.
[141] M.A. El-Sayed, Some interesting properties of metals confined in time and nanometer space of different shapes, Acc. Chem. Res. 34 (2001) 257–264.
[142] E.A. Deliyanni, E.N. Peleka, K.A. Matis, Modeling the sorption of metal ions from aqueous solution by iron-based adsorbents, J. Hazard. Mater. 172 (2009) 550–558.
[143] T. Pradeep, Anshup, Noble metal nanoparticles for water purification: a critical review, Thin Solid Films 517 (2009) 6441–6478.
[144] B. Pan, B. Pan, W. Zhang, L. Lv, Q. Zhang, S. Zheng, Development of polymeric and polymer-based hybrid adsorbents for pollutants removal from waters, Chem. Eng. J. 151 (2009) 19–29.
[145] A.R. Mahdavian, M.A.-S. Mirrahimi, Efficient separation of heavy metal cations by anchoring polyacrylic acid on superparamagnetic magnetite nanoparticles through surface modification, Chem. Eng. J. 159 (2010) 264–271.
[146] X. Zhao, L. Lv, B. Pan, W. Zhang, S. Zhang, Q. Zhang, Polymer-supported nanocomposites for environmental application: a review, Chem. Eng. J. 170 (2011) 381–394.
[147] P.R. Grossl, D.L. Sparks, C.C. Ainsworth, Rapid kinetics of Cu(II) adsorption/desorption on goethite, Environ. Sci. Technol. 28 (1994) 1422–1429.
[148] Y.-H. Chen, F.-A. Li, Kinetic study on removal of copper(II) using goethite and hematite nano-photocatalysts, J. Colloid Interface Sci. 347 (2010) 277–281.
[149] J. Hu, G. Chen, I. Lo, Selective removal of heavy metals from industrial wastewater using maghemite nanoparticle: performance and mechanisms, J. Environ. Eng. 132 (2006) 709–715.
[150] X. Ma, Y. Wang, M. Gao, H. Xu, G. Li, A novel strategy to prepare ZnO/PbS heterostructured functional nanocomposite utilizing the surface adsorption property of ZnO nanosheets, Catal. Today 158 (2010) 459–463.
[151] C.-Y. Cao, Z.-M. Cui, C.-Q. Chen, W.-G. Song, W. Cai, Ceria hollow nanospheres produced by a template-free microwave-assisted hydrothermal method for heavy metal ion removal and catalysis, J. Phys. Chem. C 114 (2010) 9865–9870.
[152] K.E. Engates, H.J. Shipley, Adsorption of Pb, Cd, Cu, Zn, and Ni to titanium dioxide nanoparticles: effect of particle size, solid concentration, and exhaustion, Environ. Sci. Pollut. Res. 18 (2011) 386–395.
[153] A. Afkhami, M. Saber-Tehrani, H. Bagheri, Simultaneous removal of heavy-metal ions in wastewater samples using nano-alumina modified with 2,4-dinitrophenylhydrazine, J. Hazard. Mater. 181 (2010) 836–844.
[154] L. Cumbal, A.K. SenGupta, Arsenic removal using polymer-supported hydrated iron(III) oxide nanoparticles: role of donnan membrane effect, Environ. Sci. Technol. 39 (2005) 6508–6515.
[155] M. Jang, W. Chen, F.S. Cannon, Preloading hydrous ferric oxide into granular activated carbon for arsenic removal, Environ. Sci. Technol. 42 (2008) 3369–3374.
[156] K.L. Chen, S.E. Mylon, M. Elimelech, Enhanced aggregation of alginate-coated iron oxide (hematite) nanoparticles in the presence of calcium, strontium, and barium cations, Langmuir 23 (2007) 5920–5928.
[157] B.Ø. Hansen, P. Kwan, M.M. Benjamin, C.-W. Li, G.V. Korshin, Use of iron oxide-coated sand to remove strontium from simulated hanford tank wastes, Environ. Sci. Technol. 35 (2001) 4905–4909.
[158] J.M. Zachara, S.C. Smith, L.S. Kuzel, Adsorption and dissociation of Co-EDTA complexes in iron oxide-containing subsurface sands, Geochim. Cosmochim. Acta 59 (1995) 4825–4844.
[159] E. Eren, Removal of lead ions by Unye (Turkey) bentonite in iron and magnesium oxide-coated forms, J. Hazard. Mater. 165 (2009) 63–70.
[160] E. Eren, A. Tabak, B. Eren, Performance of magnesium oxide-coated bentonite in removal process of copper ions from aqueous solution, Desalination 257 (2010) 163–169.
[161] P.-Y. Hu, Y.-H. Hsieh, J.-C. Chen, C.-Y. Chang, Characteristics of manganese-coated sand using SEM and EDAX analysis, J. Colloid Interface Sci. 272 (2004) 308–313.
[162] S.-M. Lee, W.-G. Kim, C. Laldawngliana, D. Tiwari, Removal behavior of surface modified Sand for Cd(II) and Cr(VI) from aqueous solutions, J. Chem. Eng. Data 55 (2010) 3089–3094.
[163] S. Zhang, F. Cheng, Z. Tao, F. Gao, J. Chen, Removal of nickel ions from wastewater by Mg(OH)₂/MgO nanostructures embedded in Al₂O₃ membranes, J. Alloys Compd. 426 (2006) 281–285.
[164] J. Otsu, Y. Oshima, New approaches to the preparation of metal or metal oxide particles on the surface of porous materials using supercritical water: development of supercritical water impregnation method, J. Supercrit. Fluids 33 (2005) 61–67.
[165] B. Pan, H. Qiu, B. Pan, G. Nie, L. Xiao, L. Lv, W. Zhang, Q. Zhang, S. Zheng, Highly efficient removal of heavy metals by polymer-supported nanosized hydrated Fe(III) oxides: behavior and XPS study, Water Res. 44 (2010) 815–824.
[166] Q. Su, B. Pan, B. Pan, Q. Zhang, W. Zhang, L. Lv, X. Wang, J. Wu, Q. Zhang, Fabrication of polymer-supported nanosized hydrous manganese dioxide (HMO) for enhanced lead removal from waters, Sci. Total Environ. 407 (2009) 5471–5477.
[167] S. Wan, X. Zhao, L. Lv, Q. Su, H. Gu, B. Pan, W. Zhang, Z. Lin, J. Luan, Selective adsorption of Cd(II) and Zn(II) ions by nano-hydrous manganese dioxide (HMO)-encapsulated cation exchanger, Ind. Eng. Chem. Res. 49 (2010) 7574–7579.
[168] L. Agouborde, R. Navia, Heavy metals retention capacity of a non-conventional sorbent developed from a mixture of industrial and agricultural wastes, J. Hazard. Mater. 167 (2009) 536–544.
[169] A.Z.M. Badruddoza, A.S.H. Tay, P.Y. Tan, K. Hidajat, M.S. Uddin, Carboxymethyl-β-cyclodextrin conjugated magnetic nanoparticles as nano-adsorbents for removal of copper ions: synthesis and adsorption studies, J. Hazard. Mater. 185 (2011) 1177–1186.
[170] S. Lazarević, I. Janković-Častvan, V. Djokić, Z. Radovanović, D. Janaćković, R. Petrović, Iron-modified sepiolite for Ni²⁺ Sorption from aqueous solution: an equilibrium, kinetic, and thermodynamic study, J. Chem. Eng. Data 55 (2010) 5681–5689.
[171] M.A.M. Khraisheh, Y.S. Al-degs, W.A.M. McMinn, Remediation of wastewater containing heavy metals using raw and modified diatomite, Chem. Eng. J. 99 (2004) 177–184.
[172] Y. Kikuchi, Q. Qian, M. Machida, H. Tatsumoto, Effect of ZnO loading to activated carbon on Pb(II) adsorption from aqueous solution, Carbon 44 (2006) 195–202.
[173] D. Zhang, Preparation and Characterization of Nanometer Calcium Titanate Immobilized on Aluminum Oxide and its Adsorption Capacity for Heavy Metal Ions in Water. Advanced Materials Research, Trans Tech Publ., 2011, pp. 670–673.
[174] C.H. Lai, C.Y. Chen, B.L. Wei, C.W. Lee, Adsorptive characteristics of cadmium and lead on the goethite-coated sand surface, J. Environ. Sci. Health A Tox Hazard. Subst. Environ. Eng. 36 (2001) 747–763.
[175] H. Sun, L. Cao, L. Lu, Magnetite/reduced graphene oxide nanocomposites: one step solvothermal synthesis and use as a novel platform for removal of dye pollutants, Nano Res. 4 (2011) 550–562.
[176] M. Liu, C. Chen, J. Hu, X. Wu, X. Wang, Synthesis of magnetite/graphene oxide composite and application for cobalt(II) removal, J. Phys. Chem. C 115 (2011) 25234–25240.

C. Santhosh et al./Chemical Engineering Journal 306 (2016) 1116–1137

[177] C. Santhosh, P. Kollu, S. Doshi, M. Sharma, D. Bahadur, M.T. Vanchinathan, P. Saravanan, B.-S. Kim, A.N. Grace, Adsorption, photodegradation and antibacterial study of graphene-Fe$_3$O$_4$ nanocomposite for multipurpose water purification application, RSC Advances 4 (2014) 28300–28308.

[178] S. Chella, P. Kollu, E.V.P.R. Komarala, S. Doshi, M. Saranya, S. Felix, R. Ramachandran, P. Saravanan, V.L. Koneru, V. Venugopal, S.K. Jeong, A. Nirmala, Grace, Solvothermal synthesis of MnFe$_2$O$_4$-graphene composite– investigation of its adsorption and antimicrobial properties, Appl. Surf. Sci. 327 (2015) 27–36.

[179] C. Santhosh, P. Kollu, S. Felix, V. Velmurugan, S.K. Jeong, A.N. Grace, CoFe$_2$O$_4$ and NiFe$_2$O$_4$@graphene adsorbents for heavy metal ions – kinetic and thermodynamic analysis, RSC Adv. 5 (2015) 28965–28972.

[180] S.K. Giri, N.N. Das, G.C. Pradhan, Synthesis and characterization of magnetite nanoparticles using waste iron ore tailings for adsorptive removal of dyes from aqueous solution, Colloids Surf. A 389 (2011) 43–49.

[181] B. Stephen Inbaraj, B.H. Chen, Dye adsorption characteristics of magnetite nanoparticles coated with a biopolymer poly(γ-glutamic acid), Bioresour. Technol. 102 (2011) 8868–8876.

[182] H.H. Salih, C.L. Patterson, G.A. Sorial, R. Sinha, R. Krishnan, The implication of iron oxide nanoparticles on the removal of trichloroethylene by adsorption, Chem. Eng. J. 193–194 (2012) 422–428.

[183] M. Shariati-Rad, M. Irandoust, S. Amri, M. Feyzi, F. Ja'fari, Magnetic solid phase adsorption, preconcentration and determination of methyl orange in water samples using silica coated magnetic nanoparticles and central composite design, International, Nano Lett. 4 (2014) 91–101.

[184] H. Zhu, R. Jiang, Y.-Q. Fu, J.-H. Jiang, L. Xiao, G.-M. Zeng, Preparation, characterization and dye adsorption properties of γ-Fe$_2$O$_3$/SiO$_2$/chitosan composite, Appl. Surf. Sci. 258 (2011) 1337–1344.

[185] H.-Y. Zhua, R. Jianga, L. Xiaob, W. Lib, A novel magnetically separable-Fe$_2$O$_3$/ crosslinked chitosan adsorbent: preparation, characterization and adsorption application for removal of hazardous azo dye, J. Hazard. Mater. 179 (2010) 251–257.

[186] G. Mihoc, R. Ianoş, C. Păcurariu, Adsorption of phenol and p-chlorophenol from aqueous solutions by magnetic nanopowder, Water Sci. Technol. 69 (2014) 385–391.

[187] R. Istratie, M. Stoia, C. Păcurariu, C. Locovei, Single and simultaneous adsorption of methyl orange and phenol onto magnetic iron oxide/carbon nanocomposites, Arabian J. Chem. (2016).

[188] S. Qadri, A. Ganoe, Y. Haik, Removal and recovery of acridine orange from solutions by use of magnetic nanoparticles, J. Hazard. Mater. 169 (2009) 318–323.

[189] S.-Y. Mak, D.-H. Chen, Fast adsorption of methylene blue on polyacrylic acid-bound iron oxide magnetic nanoparticles, Dyes Pigm. 61 (2004) 93–98.

[190] M.H. Liao, K.Y. Wu, D.H. Chen, Fast adsorption of crystal violet on polyacrylic acid-bound magnetic nanoparticles, Sep. Sci. Technol. 39 (2005) 1563–1575.

[191] B. Zargar, H. Parham, A. Hatamie, Fast removal and recovery of amaranth by modified iron oxide magnetic nanoparticles, Chemosphere 76 (2009) 554–557.

[192] X. Zhao, Y. Shi, T. Wang, Y. Cai, G. Jiang, Preparation of silica-magnetite nanoparticle mixed hemimicelle sorbents for extraction of several typical phenolic compounds from environmental water samples, J. Chromatogr. A 1188 (2008) 140–147.

[193] Y.C. Chang, D.H. Chen, Adsorption kinetics and thermodynamics of acid dyes on a carboxymethylated chitosan-conjugated magnetic nano-adsorbent, Macromol. Biosci. 5 (2005) 254–261.

[194] S.F. Soares, T.R. Simões, M. António, T. Trindade, A.L. Daniel-da-Silva, Hybrid nanoadsorbents for the magnetically assisted removal of metoprolol from water, Chem. Eng. J. 302 (2016) 560–569.

[195] S. Kutzner, M. Schaffer, H. Börnick, T. Licha, E. Worch, Sorption of the organic cation metoprolol on silica gel from its aqueous solution considering the competition of inorganic cations, Water Res. 54 (2014) 273–283.

[196] R. Satheesh, K. Vignesh, M. Rajarajan, A. Suganthi, S. Sreekantan, M. Kang, B.S. Kwak, Removal of congo red from water using quercetin modified α-Fe$_2$O$_3$ nanoparticles as effective nanoadsorbent, Mater. Chem. Phys. (2016).

[197] C. Muthukumaran, V.M. Sivakumar, M. Thirumarimurugan, Adsorption isotherms and kinetic studies of crystal violet dye removal from aqueous solution using surfactant modified magnetic nanoadsorbent, J. Taiwan Inst. Chem. Eng. 63 (2016) 354–362.

[198] S. Galdiero, A. Falanga, M. Vitiello, M. Cantisani, V. Marra, M. Galdiero, Silver nanoparticles as potential antiviral agents, Molecules 16 (2011) 8894–8918.

[199] A.B. Seabra, N. Durán, Nanotoxicology of metal oxide nanoparticles, Metals 5 (2015) 934–975.

[200] B. Geng, Z. Jin, T. Li, X. Qi, Kinetics of hexavalent chromium removal from water by chitosan-Fe^0 nanoparticles, Chemosphere 75 (2009) 825–830.

[201] W.L. Du, Z.R. Xu, X.Y. Han, Y.L. Xu, Z.G. Miao, Preparation, characterization and adsorption properties of chitosan nanoparticles for eosin Y as a model anionic dye, J. Hazard. Mater. 153 (2008) 152–156.

[202] W.H. Cheung, Y.S. Szeto, G. McKay, Enhancing the adsorption capacities of acid dyes by chitosan nano particles, Bioresour. Technol. 100 (2009) 1143–1148.

[203] Q. Zhang, B. Pan, S. Zhang, J. Wang, W. Zhang, L. Lv, New insights into nanocomposite adsorbents for water treatment: a case study of polystyrene-supported zirconium phosphate nanoparticles for lead removal, J. Nanopart. Res. 13 (2011) 5355–5364.

[204] X. Jin, C. Yu, Y. Li, Y. Qi, L. Yang, G. Zhao, H. Hu, Preparation of novel nano-adsorbent based on organic–inorganic hybrid and their adsorption for heavy

[205] L. Chen, T.-J. Wang, H.-X. Wu, Y. Jin, Y. Zhang, X.-M. Dou, Optimization of a Fe–Al–Ce nano-adsorbent granulation process that used spray coating in a fluidized bed for fluoride removal from drinking water, Powder Technol. 206 (2011) 291–296.

[206] F. Hashem, Adsorption of Methylene Blue from Aqueous Solutions using Fe$_3$O$_4$/Bentonite Nanocomposite, 2012.

[207] Y. Yang, S. Han, Q. Fan, S.C. Ugbolue, Nanoclay and modified nanoclay as sorbents for anionic, cationic and nonionic dyes, Text. Res. J. 75 (2005) 622–627.

[208] P. Liu, L. Zhang, Adsorption of dyes from aqueous solutions or suspensions with clay nano-adsorbents, Sep. Purif. Technol. 58 (2007) 32–39.

[209] N. Yaroshenko, V. Sazonova, O. Perlova, N. Perlova, Sorption of uranium compounds by zirconium-silica nanosorbents, Russ. J. Appl. Chem. 85 (2012) 849–855.

[210] X.G. Li, H. Feng, M.R. Huang, Strong adsorbability of mercury ions on aniline/sulfoanisidine copolymer nanosorbents, Chem. A Eur. J. 15 (2009) 4573–4581.

[211] H.S. Park, Y.C. Lee, B.G. Choi, W.H. Hong, J.W. Yang, Clean and facile solution synthesis of Iron (III)-entrapped γ-alumina nanosorbents for arsenic removal, ChemSusChem 1 (2008) 356–362.

[212] X. Ouyang, W. Li, S. Xie, T. Zhai, M. Yu, J. Gan, X. Lu, Hierarchical CeO$_2$ nanospheres as highly-efficient adsorbents for dye removal, New J. Chem. 37 (2013) 585–588.

[213] M. Mohapatra, D. Hariprasad, L. Mohapatra, S. Anand, B. Mishra, Mg-doped nano ferrihydrite—a new adsorbent for fluoride removal from aqueous solutions, Appl. Surf. Sci. 258 (2012) 4228–4236.

[214] N.N. Nassar, Kinetics, mechanistic, equilibrium, and thermodynamic studies on the adsorption of acid red dye from wastewater by γ-Fe$_2$O$_3$ nanoadsorbents, Sep. Sci. Technol. 45 (2010) 1092–1103.

[215] Y.-H. Li, S. Wang, A. Cao, D. Zhao, X. Zhang, C. Xu, Z. Luan, D. Ruan, J. Liang, D. Wu, Adsorption of fluoride from water by amorphous alumina supported on carbon nanotubes, Chem. Phys. Lett. 350 (2001) 412–416.

[216] Y.-H. Li, S. Wang, X. Zhang, J. Wei, C. Xu, Z. Luan, D. Wu, Adsorption of fluoride from water by aligned carbon nanotubes, Mater. Res. Bull. 38 (2003) 469–476.

[217] S.G. Wang, Y. Ma, Y.J. Shi, W.X. Gong, Defluoridation performance and mechanism of nano-scale aluminum oxide hydroxide in aqueous solution, J. Chem. Technol. Biotechnol. 84 (2009) 1043–1050.

[218] G. Patel, U. Pal, S. Menon, Removal of fluoride from aqueous solution by CaO nanoparticles, Sep. Sci. Technol. 44 (2009) 2806–2826.

[219] X. Zhao, J. Wang, F. Wu, T. Wang, Y. Cai, Y. Shi, G. Jiang, Removal of fluoride from aqueous media by Fe$_3$O$_4$@ Al(OH)$_3$ magnetic nanoparticles, J. Hazard. Mater. 173 (2010) 102–109.

[220] A. Bhatnagar, E. Kumar, M. Sillanpää, Nitrate removal from water by nano-alumina: characterization and sorption studies, Chem. Eng. J. 163 (2010) 317–323.

[221] E. Kumar, A. Bhatnagar, U. Kumar, M. Sillanpää, Defluoridation from aqueous solutions by nano-alumina: characterization and sorption studies, J. Hazard. Mater. 186 (2011) 1042–1049.

[222] A. Bhatnagar, M. Sillanpää, Sorption studies of bromate removal from water by nano–Al$_2$O$_3$, Sep. Sci. Technol. 47 (2012) 89–95.

[223] R. Raveendra, P. Prashanth, R.H. Krishna, N. Bhagya, B. Nagabhushana, H.R. Naika, K. Lingaraju, H. Nagabhushana, B.D. Prasad, Synthesis, structural characterization of nano ZnTiO$_3$ ceramic: an effective azo dye adsorbent and antibacterial agent, J. Asian Ceram. Soc. 2 (2014) 357–365.

[224] F. Taghizadeh, M. Ghaedi, K. Kamali, E. Sharifpour, R. Sahraie, M. Purkait, Comparison of nickel and/or zinc selenide nanoparticle loaded on activated carbon as efficient adsorbents for kinetic and equilibrium study of removal of Arsenazo (III) dye, Powder Technol. 245 (2013) 217–226.

[225] D.B. Cordes, P.D. Lickiss, F. Rataboul, Recent developments in the chemistry of cubic polyhedral oligosilsesquioxanes, Chem. Rev. 110 (2010) 2081–2173.

[226] J.S. Seo, D. Whang, H. Lee, S. Im Jun, J. Oh, Y.J. Jeon, K. Kim, A homochiral metal–organic porous material for enantioselective separation and catalysis, Nature 404 (2000) 982–986.

[227] C.H. Christensen, K. Johannsen, I. Schmidt, C.H. Christensen, Catalytic benzene alkylation over mesoporous zeolite single crystals: improving activity and selectivity with a new family of porous materials, J. Am. Chem. Soc. 125 (2003) 13370–13371.

[228] R.J. White, V. Budarin, R. Luque, J.H. Clark, D.J. Macquarrie, Tuneable porous carbonaceous materials from renewable resources, Chem. Soc. Rev. 38 (2009) 3401–3418.

[229] S.-Y. Ding, W. Wang, Covalent organic frameworks (COFs): from design to applications, Chem. Soc. Rev. 42 (2013) 548–568.

[230] A. Patra, U. Scherf, Fluorescent microporous organic polymers: potential testbed for optical applications, Chem. A Eur. J. 18 (2012) 10074–10080.

[231] M. Hartmann, S. Kullmann, H. Keller, Wastewater treatment with heterogeneous Fenton-type catalysts based on porous materials, J. Mater. Chem. 20 (2010) 9002–9017.

[232] Q. Liu, L. Wang, A. Xiao, J. Gao, W. Ding, H. Yu, J. Huo, M. Ericson, Templated preparation of porous magnetic microspheres and their application in removal of cationic dyes from wastewater, J. Hazard. Mater. 181 (2010) 586–592.

[233] F.-H. Wang, W. Jiang, Y. Fang, C.-W. Cheng, Preparation of Fe$_3$O$_4$ magnetic porous microspheres (MPMs) and their application in treating mercury-

containing wastewater from the polyvinyl chloride industry by calcium carbide method, Chem. Eng. J. 259 (2015) 827–836.

[234] H. Liu, M. Puchberger, U. Schubert, A facile route to difunctionalized monosubstituted octasilsesquioxanes, Chem. A Eur. J. 17 (2011) 5019–5023.

[235] J.C. Furgal, J.H. Jung, T. Goodson III, R.M. Laine, Analyzing structure-photophysical property relationships for isolated T8, T10, and T12 stilbenevinylsilsesquioxanes, J. Am. Chem. Soc. 135 (2013) 12259–12269.

[236] Y. Liu, W. Yang, H. Liu, Azobenzene-functionalized cage silsesquioxanes as inorganic-organic hybrid, photoresponsive, nanoscale, building blocks, Chem. A Eur. J. 21 (2015) 4731–4738.

[237] J. Wu, P.T. Mather, POSS Polymers: Physical Properties and Biomaterials Applications, 2009.

[238] J. Zhao, Y. Fu, S. Liu, Polyhedral oligomeric silsesquioxane (POSS)-modified thermoplastic and thermosetting nanocomposites: a review, Polym. Polym. Compos. 16 (2008) 483.

[239] H. Hussain, K.Y. Mya, Y. Xiao, C. He, Octafunctional cubic silsesquioxane (CSSQ)/poly (methyl methacrylate) nanocomposites: synthesis by atom transfer radical polymerization at mild conditions and the influence of CSSQ on nanocomposites, J. Polym. Sci. Part A Polym. Chem. 46 (2008) 766–776.

[240] R. Shen, H. Liu, Construction of bimodal silsesquioxane-based porous materials from triphenylphosphine or triphenylphosphine oxide and their size-selective absorption for dye molecules, RSC Adv. 6 (2016) 37731–37739.

[241] X. Liu, H. Chen, C. Wang, R. Qu, C. Ji, C. Sun, Y. Zhang, Synthesis of porous acrylonitrile/methyl acrylate copolymer beads by suspended emulsion polymerization and their adsorption properties after amidoximation, J. Hazard. Mater. 175 (2010) 1014–1021.

[242] A. Nilchi, A. Babalou, R. Rafiee, H.S. Kalal, Adsorption properties of amidoxime resins for separation of metal ions from aqueous systems, React. Funct. Polym. 68 (2008) 1665–1670.

[243] M. Zohuriaan-Mehr, A. Pourjavadi, M. Salehi-Rad, Modified CMC. 2. Novel carboxymethylcellulose-based poly (amidoxime) chelating resin with high metal sorption capacity, React. Funct. Polym. 61 (2004) 23–31.

[244] N. El-Sawy, E. Hegazy, A.E.-H. Ali, M.A. Motlab, A. Awadallah-F, Physicochemical study of radiation-grafted LDPE copolymer and its use in metal ions adsorption, Nucl. Instrum. Methods Phys. Res. Sect. B 264 (2007) 227–234.

[245] M.R. Hoffmann, S.T. Martin, W. Choi, D.W. Bahnemann, Environmental applications of semiconductor photocatalysis, Chem. Rev. 95 (1995) 69–96.

[246] C. Hu, C.Y. Jimmy, Z. Hao, P.K. Wong, Photocatalytic degradation of triazine-containing azo dyes in aqueous TiO_2 suspensions, Appl. Catal. B 42 (2003) 47–55.

[247] C. Kormann, D.W. Bahnemann, M.R. Hoffmann, Photolysis of chloroform and other organic molecules in aqueous titanium dioxide suspensions, Environ. Sci. Technol. 25 (1991) 494–500.

[248] D.F. Ollis, C.-Y. Hsiao, L. Budiman, C.-L. Lee, Heterogeneous photoassisted catalysis: conversions of perchloroethylene, dichloroethane, chloroacetic acids, and chlorobenzenes, J. Catal. 88 (1984) 89–96.

[249] Y. Yu, C.Y. Jimmy, C.-Y. Chan, Y.-K. Che, J.-C. Zhao, L. Ding, W.-K. Ge, P.-K. Wong, Enhancement of adsorption and photocatalytic activity of TiO_2 by using carbon nanotubes for the treatment of azo dye, Appl. Catal. B 61 (2005) 1–11.

[250] N. Zhang, Y. Zhang, X. Pan, M.-Q. Yang, Y.-J. Xu, Constructing ternary CdS–graphene–TiO_2 hybrids on the flatland of graphene oxide with enhanced visible-light photoactivity for selective transformation, J. Phys. Chem. C 116 (2012) 18023–18031.

[251] J. Shen, W. Huang, N. Li, M. Ye, Highly efficient degradation of dyes by reduced graphene oxide–ZnCdS supramolecular photocatalyst under visible light, Ceram. Int. 41 (2015) 761–767.

[252] P. Chen, T.-Y. Xiao, H.-H. Li, J.-J. Yang, Z. Wang, H.-B. Yao, S.-H. Yu, Nitrogen-doped graphene/ZnSe nanocomposites: hydrothermal synthesis and their enhanced electrochemical and photocatalytic activities, ACS Nano 6 (2011) 712–719.

[253] G. Xiao, X. Wang, D. Li, X. Fu, InVO 4-sensitized TiO_2 photocatalysts for efficient air purification with visible light, J. Photochem. Photobiol. A 193 (2008) 213–221.

[254] Z. Xiong, L.L. Zhang, J. Ma, X. Zhao, Photocatalytic degradation of dyes over graphene–gold nanocomposites under visible light irradiation, Chem. Commun. 46 (2010) 6099–6101.

[255] T. Shen, Z.-G. Zhao, Q. Yu, H.-J. Xu, Photosensitized reduction of benzil by heteroatom-containing anthracene dyes, J. Photochem. Photobiol. A 47 (1989) 203–212.

[256] J. Zhang, Z. Xiong, X. Zhao, Graphene–metal–oxide composites for the degradation of dyes under visible light irradiation, J. Mater. Chem. 21 (2011) 3634–3640.

[257] F. Fan, X. Wang, Y. Ma, K. Fu, Y. Yang, Enhanced photocatalytic degradation of dye wastewater using ZnO/reduced graphene oxide hybrids, Fullerenes Nanotubes Carbon Nanostruct. 23 (2015) 917–921.

[258] T. Xu, L. Zhang, H. Cheng, Y. Zhu, Significantly enhanced photocatalytic performance of ZnO via graphene hybridization and the mechanism study, Appl. Catal. B 101 (2011) 382–387.

[259] T. Kavitha, A.I. Gopalan, K.-P. Lee, S.-Y. Park, Glucose sensing, photocatalytic and antibacterial properties of graphene–ZnO nanoparticle hybrids, Carbon 50 (2012) 2994–3000.

[260] D. Fu, G. Han, Y. Chang, J. Dong, The synthesis and properties of ZnO–graphene nano hybrid for photodegradation of organic pollutant in water, Mater. Chem. Phys. 132 (2012) 673–681.

[261] X. Zhou, T. Shi, H. Zhou, Hydrothermal preparation of ZnO-reduced graphene oxide hybrid with high performance in photocatalytic degradation, Appl. Surf. Sci. 258 (2012) 6204–6211.

[262] L. Zhang, L. Du, X. Cai, X. Yu, D. Zhang, L. Liang, P. Yang, X. Xing, W. Mai, S. Tan, Role of graphene in great enhancement of photocatalytic activity of ZnO nanoparticle–graphene hybrids, Physica E 47 (2013) 279–284.

[263] M. Shanmugam, A. Alsalme, A. Alghamdi, R. Jayavel, Enhanced photocatalytic performance of the graphene-V_2O_5 nanocomposite in the degradation of methylene blue dye under direct sunlight, ACS Appl. Mater. Interfaces 7 (2015) 14905–14911.

[264] R.A. Rakkesh, D. Durgalakshmi, S. Balakumar, Nanostructuring of a GNS-V_2O_5-TiO_2 core–shell photocatalyst for water remediation applications under sun-light irradiation, RSC Adv. 5 (2015) 18633–18641.

[265] W.H. Organization, Global Report for Research on Infectious Diseases of Poverty, 2012.

[266] A.M. Allahverdiyev, E.S. Abamor, M. Bagirova, M. Rafailovich, Antimicrobial effects of TiO_2 and Ag_2O nanoparticles against drug-resistant bacteria and leishmania parasites, Future Microbiol. 6 (2011) 933–940.

[267] N. Cioffi, M. Rai, Nano-Antimicrobials, Progress and Prospects, Springer, Berlin, Germany, 2012.

[268] S. Liu, T.H. Zeng, M. Hofmann, E. Burcombe, J. Wei, R. Jiang, J. Kong, Y. Chen, Antibacterial activity of graphite, graphite oxide, graphene oxide, and reduced graphene oxide: membrane and oxidative stress, ACS Nano 5 (2011) 6971–6980.

[269] W. Shao, X. Liu, H. Min, G. Dong, Q. Feng, S. Zuo, Preparation, characterization, and antibacterial activity of silver nanoparticle-decorated graphene oxide nanocomposite, ACS Appl. Mater. Interfaces 7 (2015) 6966–6973.

[270] A.F. de Faria, D.S.T. Martinez, S.M.M. Meira, A.C.M. de Moraes, A. Brandelli, A. G. Souza Filho, O.L. Alves, Anti-adhesion and antibacterial activity of silver nanoparticles supported on graphene oxide sheets, Colloids Surf. B 113 (2014) 115–124.

[271] N.X. Dinh, N.V. Quy, T.Q. Huy, A.-T. Le, Decoration of silver nanoparticles on multiwalled carbon nanotubes: antibacterial mechanism and ultrastructural analysis, J. Nanomater. 2015 (2015) 63.

[272] N.X. Dinh, N.T. Lan, H. Lan, H. Van Tuan, N. Van Quy, V.N. Phan, T.Q. Huy, A.-T. Le, Water-dispersible silver nanoparticles-decorated carbon nanomaterials: synthesis and enhanced antibacterial activity, Appl. Phys. A 119 (2015) 85–95.

[273] G. Ghasemzadeh, M. Momenpour, F. Omidi, M.R. Hosseini, M. Ahani, A. Barzegari, Applications of nanomaterials in water treatment and environmental remediation, Front. Environ. Sci. Eng. 8 (2014) 471–482.

[274] I. Gehrke, A. Geiser, A. Somborn-Schulz, Innovations in nanotechnology for water treatment, Nanotechnol. Sci. Appl. 8 (2015) 1–17.